



Punching Shear Performance of Reinforced Concrete Slab-Column Joints with Shearhead Reinforcement

Yi Jiang^{1,2} · Yan Li¹ · Jing Zhou^{1,3}  · Weiwen Yi²

Received: 18 November 2023 / Revised: 23 April 2024 / Accepted: 24 May 2024 / Published online: 11 June 2024
© The Author(s), under exclusive licence to the Iran University of Science and Technology 2024

Abstract

The punching shear performance of reinforced concrete (RC) slab–column joints with shearhead reinforcement was investigated to optimize shearhead reinforcement design. Nine slab–column joint specimens were designed with different flange thicknesses, web thicknesses, cantilever lengths, and anchor stud sizes. The specimens were subjected to reversed static loading tests to investigate their failure history and failure modes; measure the load capacity, deformation, and strain of the joints; investigate the influence of different design combinations on the punching shear failure mode and load capacity of the joints; and elucidate their failure mechanisms. Test simulation analysis and numerical parametric analysis were conducted based on the test results. The results showed that the shearhead enhanced the punching shear performance of the slab–column joint and improved the brittleness of the punching shear failure. Installing steel section flanges and anchor studs enhanced the synergy among the longitudinal reinforcement, steel section, and concrete in the joint, and increasing the web thickness and installing flanges both improved the punching shear capacity and ductility of the joint. The installation of flanges on the web of the steel section increased the ultimate load capacity by more than 40% and increased the mid-span displacement at failure by more than twice that of the specimen without flanges and the specimen with studs. Adding anchor studs to the web of the steel section increased the ultimate punching shear capacity of the RC slab–column joint by 25%. Using anchor bolts instead of flanges improved the punching shear capacity of the joint but was not as effective in improving ductility. Increasing the flange thickness to increase the load capacity had a marginal effect; the ultimate load capacity increased by only 7% when the web area increased by 2/3, and the shearhead did not enhance punching shear capacity if the cantilever of the steel section was too short. Finally, based on the existing code, test results and numerical parametric analysis results, a method for calculating the punching shear capacity of RC slab–column joints with shearhead reinforcement was proposed.

Keywords Shearhead · Reinforced concrete slab–column joint · Punching shear capacity · Static test · Calculation method

✉ Jing Zhou
ctjzhou@scut.edu.cn

Yi Jiang
jiangyi_scut@126.com

Yan Li
202021008999@scut.edu.cn

Weiwen Yi
1085777875@qq.com

³ State Key Laboratory of Subtropical Building and Urban Science, South China University of Technology, 381 Wushan Road, Tianhe District, Guangzhou 510640, China

¹ School of Civil Engineering and Transportation, South China University of Technology, Guangzhou 510641, China

² Architectural Design and Research Institute, South China University of Technology, Guangzhou 510641, China

1 Introduction

Reinforced concrete (RC) flat slab floor systems are widely used in high-rise building structures with underground garages. However, the slab–column joints of RC flat slab floors can experience large shear forces and bending moments and thus are prone to brittle punching shear failure [1, 2]. In existing studies on slab–column joints, the punching shear capacity of the joint was enhanced by placing punching shear-resisting elements such as bent-up bars and stirrups, shear studs, and shearhead reinforcements [3–7]. In 1968, researchers at the University of London first proposed the shearhead reinforcement method [8], and static load test results indicated that the shearhead can significantly improve the punching shear capacity and brittle failure of a joint. Based on these test results, the American standard [9] prescribed the design method for slab–column joints with shearhead reinforcement. In the past decade, composite punching shear-resisting elements related to shearhead reinforcement, including flexural steel plates welded to the ends of steel section cantilevers [10] and shear studs welded to perforated steel plates [11], have been developed. The reliability of slab–column joints with shearhead reinforcement in ACI 318–10 was evaluated [12]. The influence of different steel section arrangements with the same amount of steel on the seismic performance of two-way slab–column joints was investigated [13]. It was experimentally confirmed that the punching shear capacity of an RC slab–concrete-filled steel tube (CFST) column joint with shearhead reinforcement is significantly greater than that of an ordinary RC slab–column joint [14, 15]. The influence of the cantilever length and cross-sectional dimensions of the steel section on the punching shear performance of an RC slab–CFST column joint was studied, and a model for calculating its punching shear capacity considering the influence of steel section design variables was proposed [10]. The shear transfer mechanism and influence mechanism of RC slab–steel column joints with shearhead reinforcement were investigated, and a simplified design method was proposed [16]. The concrete plastic damage model was applied to perform finite element (FE) numerical simulations of RC slab–column joints [17]. A theoretical model based on the analysis of an FE model was developed [18]. RC slab–column joints under a dynamic reciprocating load were analyzed via FE simulations [19]. The possible vertical load and reversed horizontal load on RC slabs were studied using numerical simulations [20]. In ACI 318–08 [9], an equation for the flexural capacity of a joint with shearhead reinforcement was given, but the calculation method for its punching shear capacity was not provided. China’s Code for the Design of Concrete Structures [21] provides a method and

equations for calculating the punching shear capacity of slab–column joints without stirrups or shear reinforcement, without mentioning the embedded shearhead or other punching shear-resisting elements. The design method of slab–column joints with shearhead reinforcement presented in China’s Technical Specification for Concrete Structures Prestressed with Unbonded Tendons [22] follows the method presented in ACI 318–08. Evidently, there remains a lack of relevant research and applications for this type of joint in China. At present, the research and design methods for determining the punching shear performance of RC slab–column joints with shearhead reinforcement still have room for improvement. In particular, there is a severe lack of experimental and theoretical research on the influences of the number and size of steel sections on the punching shear performance of RC slab–column joints, restricting their application in high-rise building structures with underground garages. The design of slab–column joints with shearhead reinforcement based on existing design methods may not only cause unnecessary construction waste but also introduce unexpected safety risks. To promote the application of shearhead reinforcement in RC slab–column joints, sufficient experimental verifications along with reasonable, reliable design theories and methods are needed.

In this study, based on an actual engineering project, nine RC slab–column joint specimens were designed by considering the flange thickness, web thickness, cantilever length, and auxiliary stud size of the steel section as variables, and then the specimens were subjected to static loading failure tests. The failure process and failure modes of the specimens were investigated, their punching shear performance and ductility characteristics were explored, the influence of the steel section size on the punching shear capacity was analyzed, and the design calculation equations in the existing code were examined to provide test bases and optimized solutions for the design and application of RC slab–column joints with shearhead reinforcement.

2 Overview of the Experimental Work

2.1 Specimen Design

Nine RC slab–column joint specimens with shearhead reinforcement were designed. The reinforcement and shearhead arrangement of the specimens are shown in Fig. 1 (taking specimen SC2 as an example). The flange thickness, web thickness, cantilever length, and stud specifications of the steel section are shown in Table 1. The RC slab had cross-sectional dimensions of $2000 \times 2000 \times 300$ mm, and a short RC column of

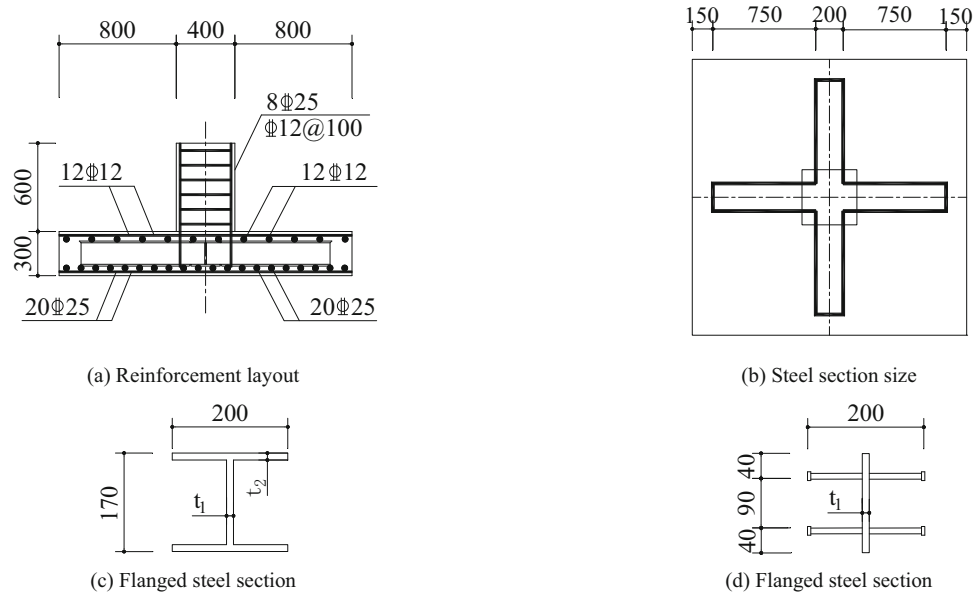


Fig. 1 Specimen dimensions, reinforcement layout and steel section information

Table 1 Specimen details

Specimen	Thickness of web t_1 (mm)	Thickness of flange t_2 (mm)	Cantilever length l (mm)	Specification of pins
SC1	–	–	–	–
SC2	12	34	1700	–
SC3	12	16	1700	–
SC4	12	6	1700	–
SC5	12	–	1700	–
SC6	12	–	1700	M16
SC7	20	16	1700	–
SC8	20	–	1700	M19
SC9	12	16	1200	–

400 × 400 mm was set at the geometric center of the slab. C45 and C40 concrete, Q345 steel, and HRB400 rebar were used to fabricate the specimens, and the reinforcement ratio of the slab section was 1.77%. Specimen SC1 was a control without a shearhead; specimens SC2–SC5 were used to investigate the influence of the flange thickness of the steel section; specimens SC5 and SC6 were used to examine the influence of the studs; specimens SC3 and SC7 were used to investigate the influence of the web thickness; specimens SC3, SC6, SC7, and SC8 were used to examine the influence of the flange and stud interchange; specimens SC6 and SC8 were used to investigate the combined influence of the web thickness and stud size; and specimens SC3 and SC9 were used to examine the shearhead cantilever length.

2.2 Test Materials

The specimens were cast in two batches. The ultimate compressive strength of the concrete cubes f_{cu} was determined according to the Standard for Test Method of Mechanical Properties on Ordinary Concrete (GB/T 50081–2002) [23]. The ultimate axial compressive strength f_c and the ultimate tensile strength f_t of the prismatic specimens were calculated according to the Standard for Test Method of Concrete Structures (GB/T 50152–2012) [24]. As shown in Table 2, the concrete strengths of specimens SC3–SC9 were lower than those of specimens SC1–SC2. The basic mechanical properties of the steel bars and sections are listed in Table 3. The shear yield strength of steel bars was determined by the dip test method, where the steel bar is placed in the fixed fixture and the tilt force is applied on one side to make it tilt to determine the shear strength.

2.3 Test Setup

For ease of description, in accordance with the placement direction of a specimen during the test loading, the upper side of the specimen (with an RC column) was defined as

Table 2 Concrete properties

Specimens	Strength grade	f_{cu} (MPa)	f_c (MPa)	f_t (MPa)
SC1–SC2	C45	45.93	34.91	3.24
SC3–SC9	C40	40.20	30.55	3.01

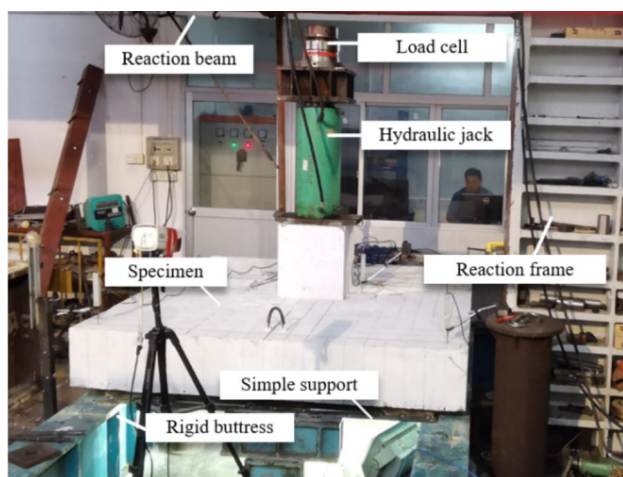
Table 3 Rebar properties

Steel type	Strength grade	Diameter (mm)	Tensile yield strength f_y (MPa)	Shear yield strength f_{vy} (MPa)	Yield strain
Reinforcement	HRB400	25	558	322	2790
		12	420	242	2100
Steel section	Q345	–	395	228	1975

the top of the slab, and the lower side of the specimen (without a column) was defined as the bottom of the slab. The test setup is illustrated in Fig. 2. Steel rollers were used to simulate simple supports on four sides, which can roughly characterize the force characteristics along inflection lines. A hydraulic jack was used to apply a vertical load to the RC short column, which worked jointly with simple supports to simulate the punching effect on an actual slab–column joint. During the test, the crack development and failure modes of the specimen were investigated, and the vertical load, slab top and bottom displacements, bottom of the slab longitudinal reinforcement strain, concrete strain, and steel section strain were recorded.

The specimens and test scheme designed in this paper are bidirectional and positively symmetric. In the test process, only the strain of key parts within 1/4 of the specimen needs to be measured to understand the global internal force evolution. However, considering the complexity of flexural and shear composite forces and the criticality of the steel shearhead, the measuring point arrangement of the steel shearhead is more comprehensive. To collect the displacement development of the top and bottom of the slab, 7 displacement meters (D1–D7) are installed, as shown in Fig. 3a. On the top of the slab, displacement meters D1 and D2 measure the vertical displacement at the support, and displacement meters D3 and

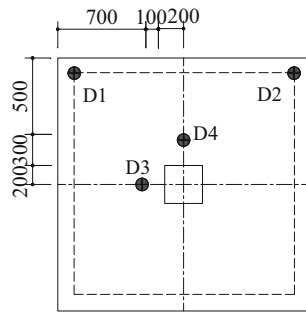
D4 measure the vertical displacement at a position 100 mm away from the side of the loading RC column edge. As shown in Fig. 3b, the displacement at the center of the slab bottom is the largest, which is measured by displacement meter D5. Displacement meters D6 and D7 measure the vertical displacement 300 mm away from the loading RC column edge, displacement meters D3 and D4, as well as D6 and D7, can be compared with each other, and the displacement development from the edge to the center of the slab can be understood by displacement meters D5, D4 (D3) and D6 (D7). The strain at the loading RC column edge and 300 mm away from the column edge is mainly collected for longitudinal steel bars. Ten measuring points (R1–R10) are arranged at the bottom of the slab, and 10 measuring points (R11–R20) are arranged on the top of the slab to measure the strain development of the bidirectional steel bars. The strain collection of concrete can only be limited to before concrete cracking, which is mainly to confirm the failure mode of the specimen, and the number of arrangements is small. Four measuring points (C1–C4) are arranged on the top of the slab, and 6 measuring points (C5–C10) are arranged on the bottom of the slab to measure the strain development of the two-way concrete before cracking. The section steel strain is a key concern and has an important influence on the analysis and judgment of the effect of the section steel shearhead. Therefore, 8 measuring points (S1–S8) are arranged on the upper flange of the section steel, 8 measuring points (S9–S16) are on the lower flange of the section steel, and 6 measuring points (S17–S22) are on the web of the section steel to investigate the development of internal forces in both directions. Figure 3 shows the arrangement of the measurement points, with the numbers in parentheses denoting the measurement points on the lower flange of the steel section.

**Fig. 2** Test setup

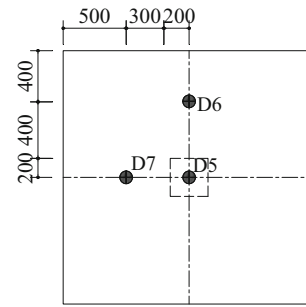
3 Failure of the Tested Specimens

3.1 Failure Process and Failure Modes

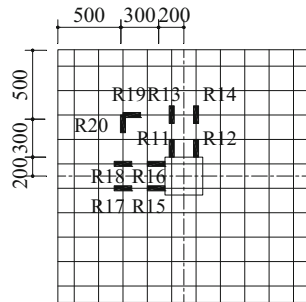
The parameters (load and displacement) at the characteristic points during the test are shown in Table 4. The displacements are the mid-span displacements measured by



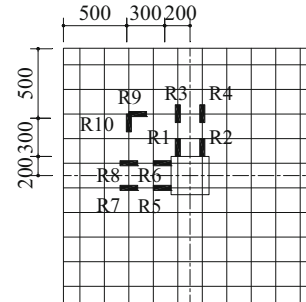
(a) Displacement measurement points on the top of the slab



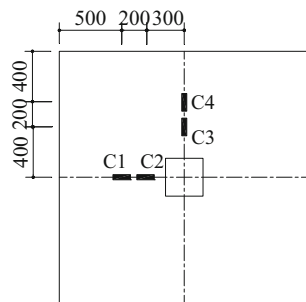
(b) Displacement measurement points at the bottom of the slab



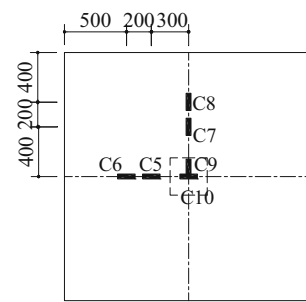
(c) Longitudinal reinforcement strain measurement points on the top of the slab



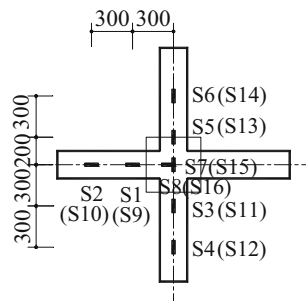
(d) Longitudinal reinforcement strain measurement points at the bottom of the slab



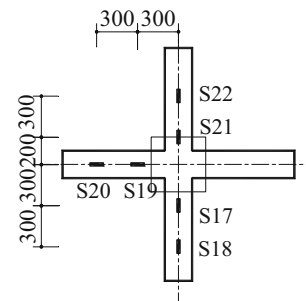
(e) Concrete strain measurement points on the top of the slab



(f) Concrete strain measurement points at the bottom of the slab



(g) Measurement points on the upper flange of the steel section



(h) Measurement points on the web of the steel section

Fig. 3 Layout of the measurement points

D5 at the bottom of the slab. Figure 4 shows the crack pattern at the bottom of the slab for each specimen after loading. The crack development and failure process of the

slab–column joint specimens was roughly divided into the following stages: first, circumferential punching shear cracks appeared 300–400 mm from the edge of the column

Table 4 Test results at characteristic points

Specimen	Cracking point		Ultimate point		Average dip angle (°)	Failure mode
	Load F_{cr} (kN)	Deflection (mm)	Load F_u (kN)	Deflection (mm)		
SC1	650	1.2	3036	6.8	–	punching-shear
SC2	2500	3.0	5079	17.6	–	flexural–punching shear
SC3	1780	3.9	3555	22.2	–	flexural
SC4	1100	2.5	3252	21.1	25.9	flexural
SC5	900	1.4	2336	5.9	–	flexural–punching shear
SC6	1380	3.7	3137	8.1	26.6	flexural–punching shear
SC7	1540	4.0	3807	20.5	–	flexural
SC8	840	1.8	2807	8.7	27.9	flexural
SC9	800	2.2	2667	11.2	–	punching-shear

on the bottom of the slab; the circumferential cracks gradually coalesced to form a main circumferential crack, which developed toward the top of the slab to form a punching cone, while radial cracks radiating to the four corners of the slab appeared around the main circumferential crack; abrupt displacement occurred near the ultimate capacity, and the RC column was punched downward into the slab along column edges; and finally, the loading was stopped due to concrete crushing near the column edges or in the support region.

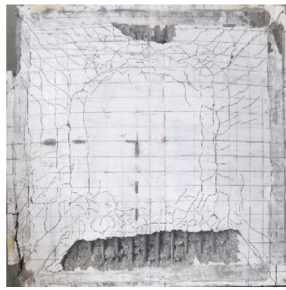
The test phenomena of specimens SC1–SC9 were essentially similar in the initial stage of loading when the deformation of the specimens was very small, and the bond between the steel section and concrete ensured that the two worked together. When the load reached 0.35–0.5 F_u (F_u was the ultimate load), the initial cracks around the column appeared on the concrete surface at the bottom of the slabs of specimens SC1–SC8 at 300–400 mm from the edge of the column, and the initial circumferential cracks in specimen SC9 were farther from the column center because its steel section had a shorter cantilever than those in the other specimens. When the load reached approximately 0.6 F_u , the stress in the lower flange of the steel section and in the web increased at an accelerated rate. As the load continued to increase, the cracks at the bottom of the slab increased and propagated, and the circumferential cracks developed to form an obvious main crack. Moreover, a small number of radial cracks gradually formed along the diagonals of the slab centered on the column outside the main circumferential crack. Near the ultimate load F_u , the width of the circumferential cracks in specimens SC1, SC5, and SC9 increased significantly to form a punching cone that penetrated the slab, and the radial flexural cracks in specimens SC3, SC4, SC7, and SC8 extended inward from outside the main circumferential crack to the center of the bottom of the slab. As the specimens failed, the end of the RC column punched into the slab, crushing the concrete of the slab at

the edges of the RC column. The shearhead played a role in restraining the development of the circumferential and radial cracks, gradually sharing the internal bending and shear forces released by the cracked concrete and restraining the tensile and compressive deformation of the concrete, thus delaying the formation and development of the punching cone.

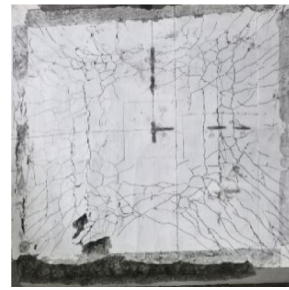
3.2 Section-Cutting Plane Analysis

To investigate the internal crack pattern due to the punching shear failure cone, the RC slabs of specimens SC4, SC6, and SC8 were cut open 500 mm from the column edge after the test. The section-cutting planes are shown in Fig. 5.

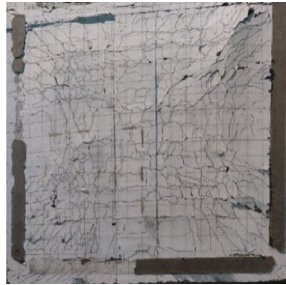
In all three specimens, there was a clear concrete fracture zone at the longitudinal reinforcement at the bottom of the slab. The fracture zone included a horizontal crack approximately 1600–1700 mm long, with dislocation slip between the longitudinal reinforcement and the concrete. At the two lower ends of the section-cutting plane, oblique cracks developed horizontally along the upper surface of the longitudinal reinforcement for approximately 300–400 mm, a phenomenon related to the yield range and dowel effect of the longitudinal reinforcement. The cracks were “concave,” and the angle between the line connecting the punching oblique crack and the initial intersection of the longitudinal reinforcement at the bottom and the top of the slab and the horizontal plane was defined as the oblique crack inclination angle [25], as shown in Table 4. The crack pattern observations from the section-cutting planes indicated that the oblique crack patterns in the specimens with shearhead reinforcement were relatively gentle compared to the punching oblique crack patterns in the RC slab–column joint specimen without a shearhead (assumed to be 45° in GB50010-2010) [21]. Based on the angle of the oblique cracks and the cracks at the bottom of the slab, the



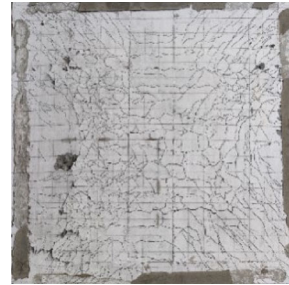
(a) SC1



(b) SC2



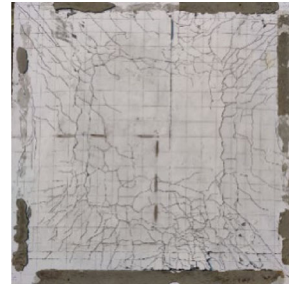
(c) SC3



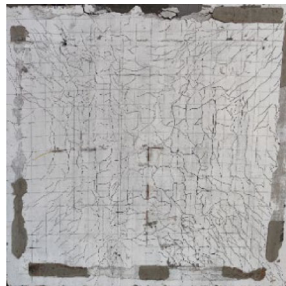
(d) SC4



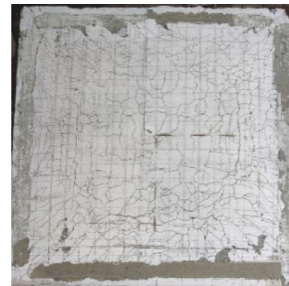
(e) SC5



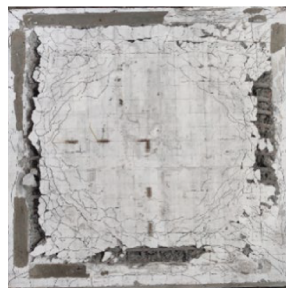
(f) SC6



(g) SC7



(h) SC8



(i) SC9

Fig. 4 Cracks at the bottom of the slab

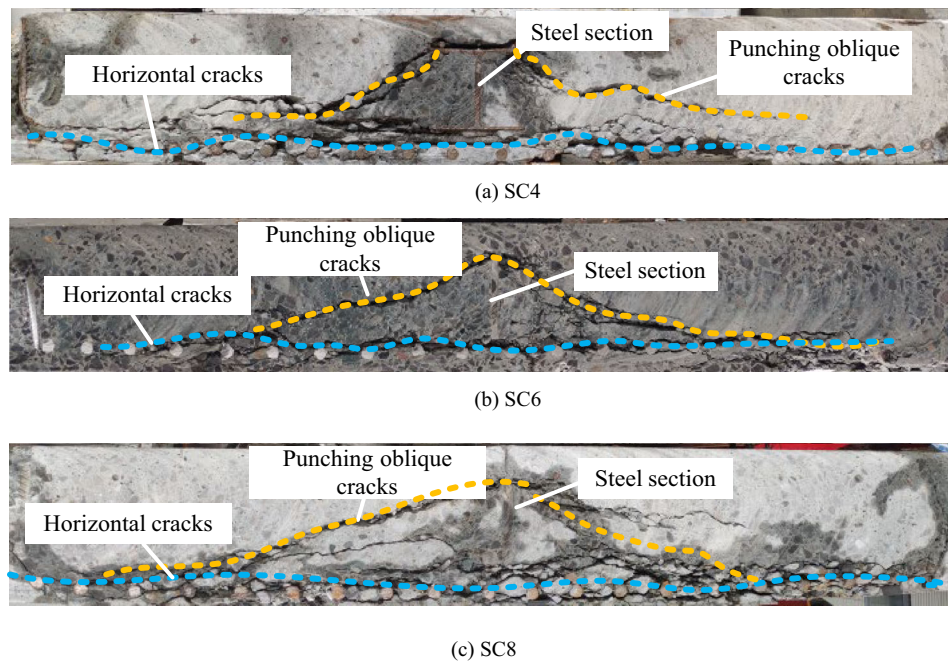


Fig. 5 Crack patterns in the section-cutting planes

punching oblique cracks all crossed the steel section to varying degrees, indicating that the embedded shearhead improves the punching shear capacity of a slab–column joint and inhibits the rapid development of the punching plane.

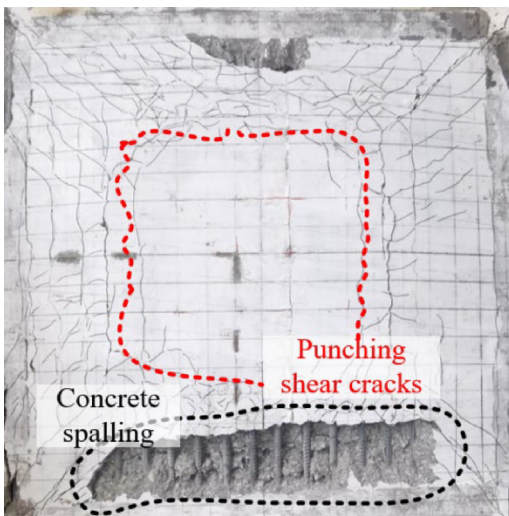
3.3 Failure Modes

To date, there has been no clear criterion for distinguishing between the punching shear failure mode and the flexural failure mode of RC slab–column joints. According to the criterion given in the literature [26], specimens that form a plastic fracture zone at the bottom of the slab are defined as flexural failure specimens, specimens that form a main circumferential crack are defined as punching shear failure specimens, and those in between are defined as flexural–punching shear failure specimens. On this basis, the failure modes of nine specimens are determined (Table 4), as shown in Fig. 6.

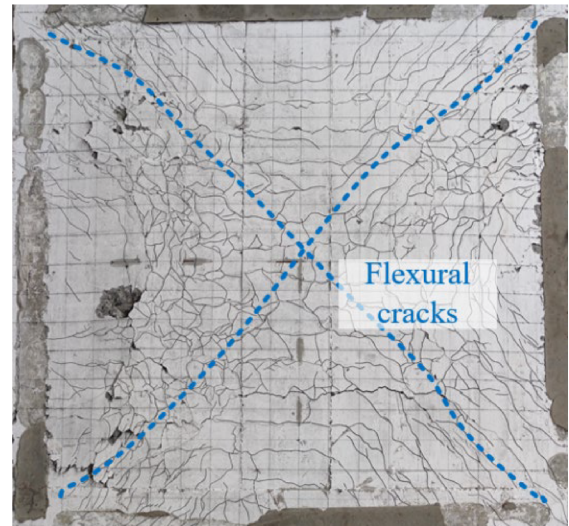
Specimen SC1 is compared with specimens SC2–SC9 to investigate the effect of the shearhead. Specimen SC1, which was not equipped with shearhead reinforcement, formed through-punching shear cracks at the bottom of the slab without flexural cracks extending into the main circumferential crack, suggesting a typical punching failure mode and a significantly low punching shear capacity.

The influence of the flange thickness of the shearhead on the failure mode is investigated by comparing specimens SC2–SC5. When the flange thickness was within a certain range (specimens SC3 and SC4), the slab–column joints

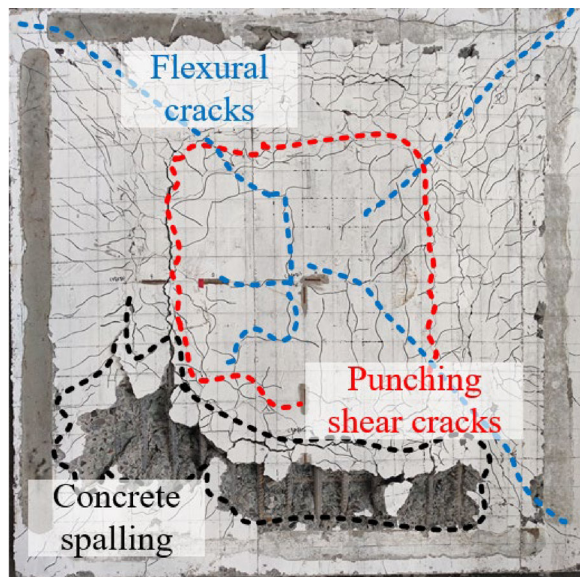
underwent flexural failure; when the ultimate capacity was reached, the deformation of the slab increased, and there was a high stress in the longitudinal reinforcement at the bottom of the slab; the longitudinal reinforcement and the shearhead jointly resisted bending and punching. When the flange thickness was too great (specimen SC2), the specimen experienced flexural–punching shear failure, which is between flexural failure and punching shear failure. This failure occurs because a thicker flange provides a higher flexural stiffness; hence, the shearhead is subjected to more bending moments than the concrete, resulting in fewer flexural cracks in the concrete at the bottom of the slab and a tendency for the failure mode to be punching shear failure. However, considering the ultimate capacity of specimen SC2, the thickened flange still played a role in enhancing the punching shear capacity. When the shearhead was not designed with flanges (specimen SC5), the failure mode changed from flexural failure to flexural–punching shear failure, and the capacity and deformation of the specimen were significantly lower than those of specimens reinforced by the shearhead with flanges or studs. These results occurred because it was difficult for the steel section without flanges to work together with the slab concrete and longitudinal reinforcement, and thus the concrete in the compression zone was crushed rapidly, resulting in local failure; the flexural and shear capacities of the flange-free steel section itself were relatively reduced. The above phenomena indicate that the punching shear capacity of a slab–column joint is not independent of



(a) Punching shear failure



(b) Flexural failure



(c) Flexural–punching shear failure

Fig. 6 Typical failure modes

the flexural capacity but is the result of the combined action of the flexural and shear capacities.

The influences of the stud diameter and web thickness were investigated by comparing specimens SC5, SC6, and SC8. The installation of studs on the web of the steel section (specimen SC6) improved the cracking and spalling of the concrete, indicating that the studs help to maintain the integrity of the steel and the concrete, which results in better synergy between the two in resisting punching shear and addresses the problem that webs alone cannot fully

provide the required shear resistance. A comparison of specimens SC6 and SC8 reveals that the failure mode of the specimens changed from flexural–punching shear failure to flexural failure by appropriately thickening the web and increasing the stud diameter, indicating that changing the web thickness and the restraining effect changes the failure mode.

Specimens SC4 and SC6 were compared with specimens SC7 and SC8 to investigate the influence of flange and stud interchange. Specimens SC4 and SC7, which had

flanged steel sections, underwent flexural failure. In contrast, specimens SC6 and SC8, which had studs instead of flanges, experienced flexural failure and flexural–punching shear failure, respectively; had fewer flexural cracks than did the specimens with flanged sections; and exhibited little deformation of the slab when the ultimate load was reached. This comparison indicates that both flanges and studs help to improve the synergistic action of the steel section, longitudinal reinforcement, and concrete to delay brittle punching shear failure, and the use of flanges outperforms the use of studs.

A comparison of specimens SC3 and SC9 was carried out to investigate the influence of the cantilever length of the steel section. Specimen SC9, with a shorter cantilever length of the shearhead, underwent punching shear failure, and the extent of the circumferential punching shear cracking at the bottom of the slab was significantly greater than that of the other specimens, with the punching cone exceeding the cantilever tip of the steel section, indicating that the shorter cantilever of the steel section allows the punching oblique crack to propagate outward along the cantilever to resist the punching action [27].

In general, when the flexural strength provided by the shearhead was lower than its shear strength (e.g., specimens SC4 and SC6), the RC slab tended to undergo flexural failure, and the longitudinal reinforcement at the bottom of the slab yielded or nearly yielded. When the flexural strength provided by the longitudinal reinforcement or steel section is greater than the shear strength (e.g., specimen SC2), although the RC slab fails with the formation of a punching cone, the tensile reinforcement at the bottom of the slab does not reach the yield state, the longitudinal reinforcement induces a certain dowel effect, which inhibits the expansion of cracks, and the shearhead shares a large portion of the internal force until the concrete at the top of the slab is crushed. Therefore, specimens with embedded shearhead reinforcement, regardless of whether they undergo flexural failure or punching shear failure, have an improved deformation capacity to a certain extent, which is clearly different from that of ordinary RC slab–column joints that undergo brittle punching shear failure.

4 Analysis and Discussion of the Test Results

4.1 Load–Displacement Curves

The test results are analyzed to evaluate the deformation capacity and ductility of the specimens using two indicators, namely, the mid-span displacement when the ultimate load is reached and the unloading gradient of the relative deformation after the ultimate load is reached. The smaller

the unloading gradient is, the better the ductility. Conversely, the larger the unloading gradient is, the poorer the ductility, which is reflected in the load–displacement curve as an abrupt drop after the peak point.

The load–displacement curves of the nine slab–column joint specimens are shown in Fig. 7. Before the concrete cracks, the slope of the load–displacement curve remains essentially constant; after entering the plastic stage, the slope of the curve decreases until a significant change in slope is reached. Near the ultimate load, except for the load capacity of control specimen SC1, which suddenly decreases, the capacity of each specimen with an embedded shearhead decreases gradually, and the deformation capacity increases significantly until the specimen fails completely, exhibiting good plastic deformation capacity. The plastic deformation segment of the load–displacement curve of specimens SC2–SC8 with an embedded shearhead is relatively flat and does not show abrupt changes, while the load–displacement curves of specimens SC1 and SC9, which experienced punching shear failure, decrease rapidly.

Figure 7a compares the results of specimen SC1 with those of specimens SC2 and SC5 to examine the contribution of the embedded shearhead to the punching shear capacity and deformation capacity of the slab–column joint. Under the same conditions, compared with SC1, SC2 was embedded with shearhead reinforcement, and as a result, its ultimate load capacity increased by 67.3%, and its mid-span displacement at failure increased by 158.8%. The ultimate load capacity of specimen SC5 was relatively small due to its relatively low concrete strength. After reaching the ultimate load, the curve of specimen SC1 drops abruptly, indicating poor ductility, while the curves of specimens SC2 and SC5 are flat, indicating gradual unloading. The above comparison indicates that the embedded shearhead as a punching shear-resisting element not only improves the punching shear capacity of the slab–column joint but also increases the plastic deformation capacity and ductility of the specimen and changes its failure mode.

Figure 7b shows the load–displacement curves of specimens SC2–SC5. In particular, the flange thickness of the steel section increased from 6 mm in SC4 to 16 mm in SC3, and correspondingly, the ultimate capacity of the specimen increased by 9.3%. Compared with that of SC5, which did not have a flange, the ultimate load capacity of SC4 increased by 39.2%, and the corresponding mid-span displacement when the ultimate load was reached increased by 255.8%. These results indicate that the shear and flexural stiffnesses provided by the steel section flanges enabled the section web to have a greater shear capacity than that of the shearhead without a flange, thereby

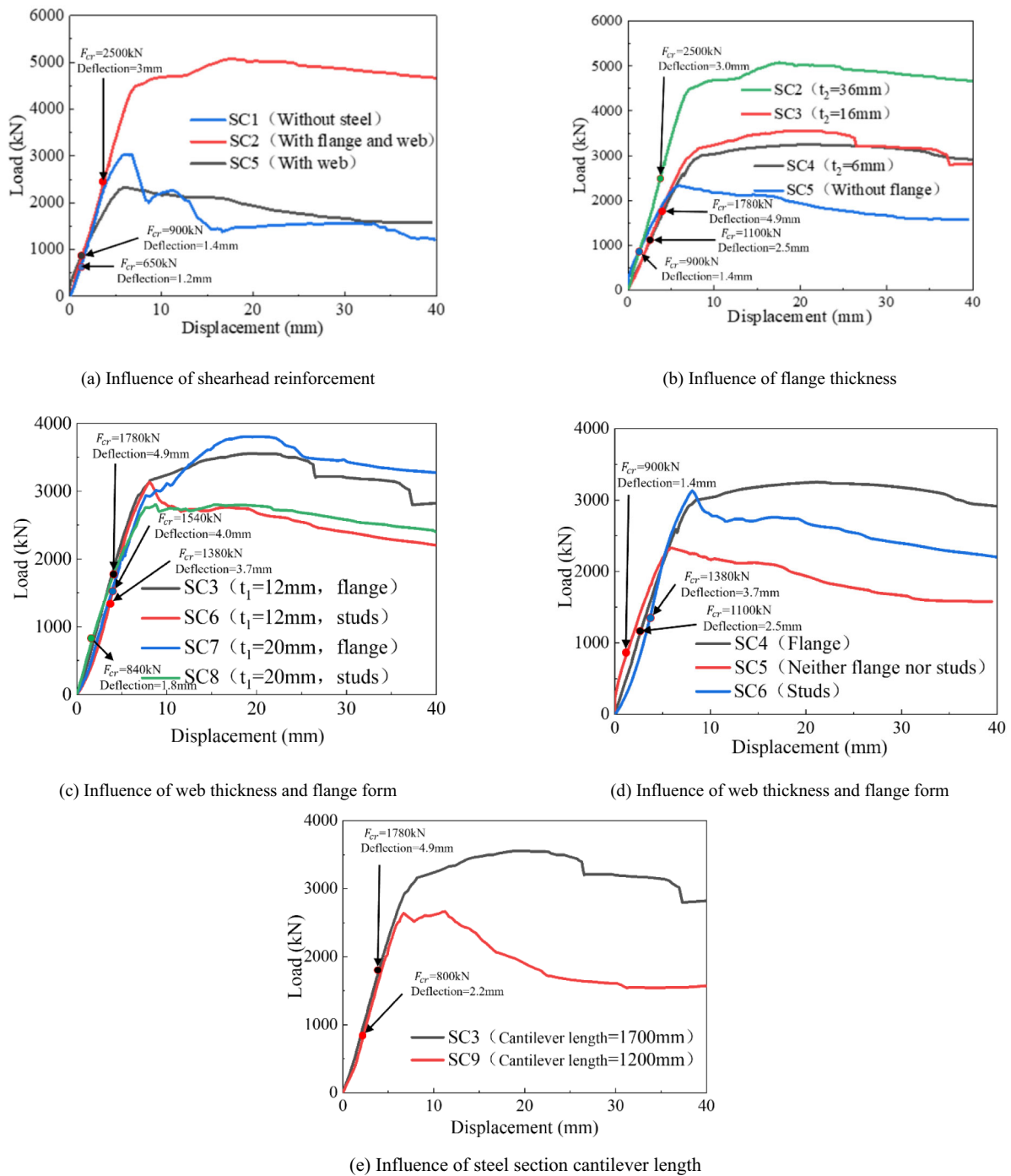


Fig. 7 Load–displacement curves of the specimens

significantly improving the punching shear capacity and deformation ductility of the slab–column joint.

Figure 7c compares the load–displacement curves of specimens SC3, SC6, SC7, and SC8. Compared with that of specimen SC3, the web thickness of specimen SC7 increased from 12 to 20 mm, and the ultimate load capacity increased by 7.1%. The web is the main component of the shearhead for shear resistance, and the change in its net

cross-sectional area directly influences the punching shear performance of the slab–column joint. Specimens SC6 and SC8, which were obtained by using studs instead of flanges in specimens SC3 and SC7, respectively, had 11.8% and 26.3% lower load capacities, respectively, and 61.6% and 60.8% lower corresponding mid-span displacements at failure, respectively, indicating that the flexural (shear) stiffness of the slab and the deformation capacity of the

specimen are significantly reduced by replacing the continuous section flanges with studs. In particular, the ultimate load capacity of specimen SC8 was lower than that of specimen SC6, which is possibly attributed to an accidental error caused by the lagging mechanism of the synergistic effect of the steel section and studs, a topic to be further investigated.

Figure 7d compares the results of specimens SC4, SC5, and SC6 to investigate the difference between the influences of flanges and studs. On the basis of specimen SC5, specimen SC6 was obtained by adding studs, and the ultimate load capacity increased by 25.5%, while the mid-span displacements of the two specimens when reaching the ultimate load were similar. Specimen SC4 was obtained by adding flanges, and as a result, the ultimate load capacity increased by 39%, and the corresponding mid-span displacement increased from 5.9 mm to 21.1 mm. These results indicate that both the studs and flanges were conducive to the resistance of the slab–column joint to the bending moment and punching shear and that the use of steel section flanges was more beneficial for improving the deformation capacity of the specimen.

Figure 7e compares the results of specimens SC3 and SC9 to examine the influence of cantilever length. The steel cantilever of specimen SC9 was reduced by 500 mm, and as a result, the ultimate load capacity was reduced by 25.0%, and the corresponding mid-span displacement at failure was reduced by 49.5%. Based on the crack pattern at the bottom of the slab, as the steel section cantilever was shortened, the punching cone expanded from the tip of the steel section cantilever, and the punching cone surface did not pass through the steel section; hence, the steel section did not provide shear or flexural resistance. For this reason, specimen SC9 underwent punching shear failure, similar to specimen SC1, which had no shearhead.

4.2 Deformation

The displacements at the bottom and top of the slab did not change completely or synchronously during the test. The deflection curves of the specimens obtained from the displacement measurement points at the bottom and top of the slab are shown in Fig. 8. The changes in the deflection curves of specimens SC2–SC8 can be divided into two stages: (1) before concrete cracking, the displacements of different measurement points developed uniformly, and the deflection increased essentially linearly at each loading level; (2) after the displacement of the central measurement point reached approximately 5 mm, there was a significant difference in the increase in the values of the displacement measurement points at the same position between the bottom and top of the slab, with relatively small changes in the displacement of the top of the slab and large changes in

the displacement of the bottom of the slab. These results indicate that damage occurred inside the RC slab, mainly through the extension and development of oblique cracks in the concrete at a large deflection, bond slip between the concrete and the steel, and many cracks on the concrete surface in tension.

Examining the specimen parameters, specimen SC1 (without a shearhead), specimen SC5 (with shearhead reinforcement that had only a web), and specimens SC6 and SC8 (with studs instead of flanges) had significantly reduced deflection at the center of the RC slab at the ultimate load compared to specimens SC2, SC3, SC4, and SC7, respectively, indicating that the embedded shearhead with flanges is beneficial for enhancing the deformation capacity of the slab, improving the deformation ductility, and thus preventing brittle punching shear failure of the slab–column joint.

4.3 Concrete Strain

The variation in the concrete strain in the compression zone of each specimen was essentially the same, and a typical concrete strain–load curve is shown in Fig. 9. The concrete strain in the tension zone at the bottom of the slab cracked, and the concrete strain in the compression zone at the top of the slab increased with increasing load. When the load reached approximately 60% to 80% of the ultimate load, the concrete strain at the radial measurement points decreased instead, and the phenomenon of concrete strain unloading occurred. The maximum strain of the concrete in the compression zone at the top of the slab in each specimen was generally smaller than the concrete ultimate compressive strain of $-3300 \mu\epsilon$. Table 5 lists the measurement points where the unloading phenomenon occurred in each specimen and the corresponding load percentage when the unloading phenomenon first occurred. The radial strain of the concrete closest to the column edge increased the most with increasing load, and the concrete radial strain unloading phenomenon was prominent, while the strain unloading amplitude at the measurement points far from the column edge was low.

Strain unloading occurred at most (69.6%) of the radial measurement points in the compression zone, and the strain unloading at different measurement points of the same specimen occurred closely in time. The concrete near the column edges and column corners of the slab–column joint was in a bidirectional compressive state because, due to the local bending of the compression zone, the concrete near the column had a local positive curvature, which resulted in the unloading and decompression of the concrete on the surface near the column [28]. The phenomenon of strain unloading indicates that with the development of the main circumferential punching shear crack in the specimen, the

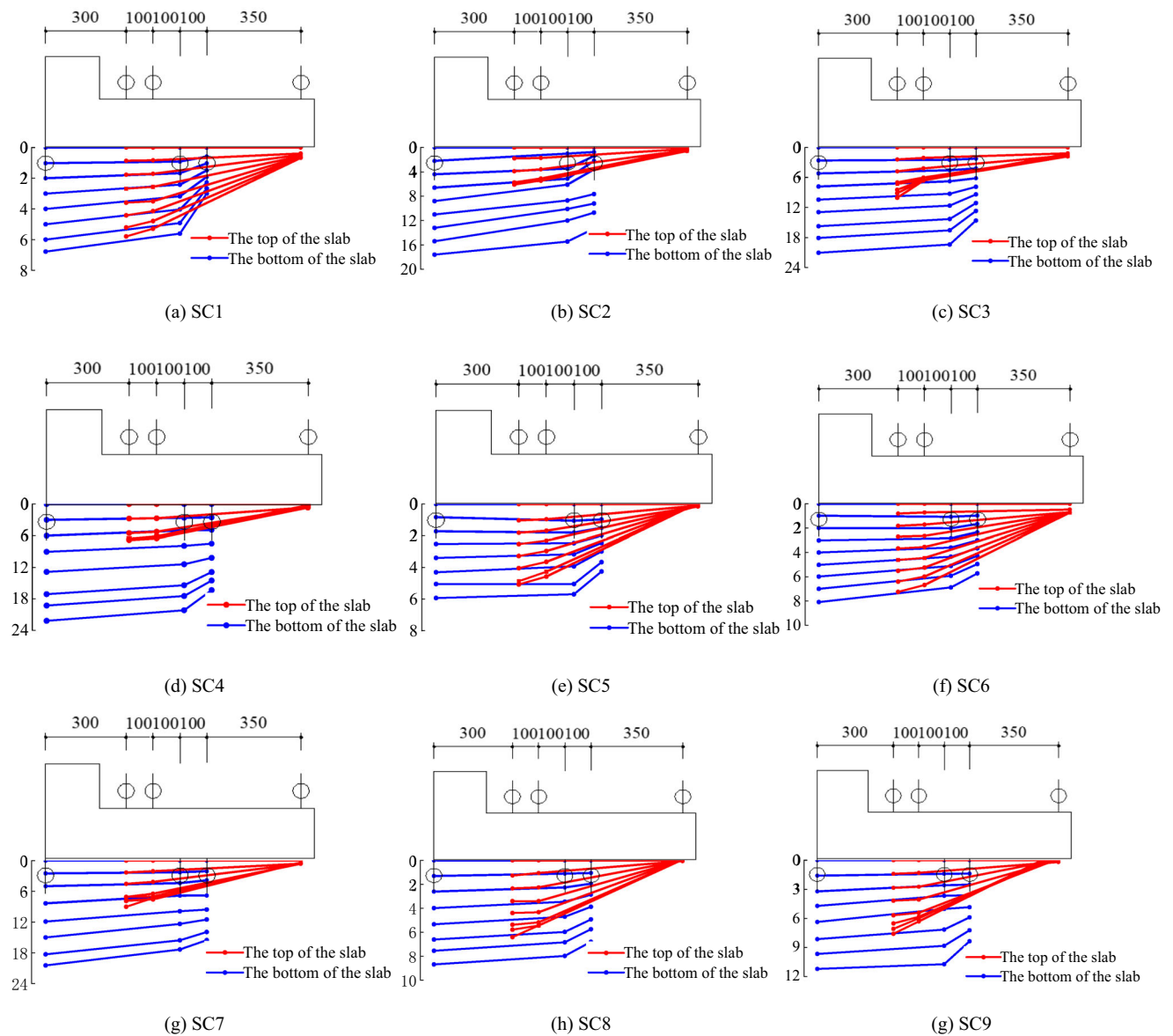


Fig. 8 Deflection curves of the RC slab

stress transfer path changes under the influence of factors such as the change in the elastic modulus of the concrete in the compression zone after damage, the redistribution of stresses of the concrete in bidirectional compression, and the reinforcing effect of the shearhead.

The concrete strain in the tension zone at the bottom of the slab varied among the specimens. As the test load increased, flexural cracks appeared in the center of the bottom of the slab in specimens SC3–SC8, and the tensile strain in the concrete at the bottom of the slab increased rapidly. The concrete strain at the center of the bottom of the slab in specimens SC1, SC2 and SC9 was always small, indicating that there were essentially no flexural cracks at the center of the bottom of the slab and that the specimens

tended to undergo punching shear failure rather than flexural failure.

4.4 Reinforcement strain

The strain of the tensile longitudinal reinforcement at the bottom of the slab is analyzed to examine the synergistic effect of the rebar and steel section. The strain values of the longitudinal reinforcement in specimens SC2–SC8 were essentially similar in all stages of development, and typical strain–load curves are shown in Fig. 10. Before the concrete cracked, a very small tensile strain was generated in the longitudinal reinforcement at the bottom of the slab, and a small amplitude of compressive strain occurred at some measurement points, which was caused by the

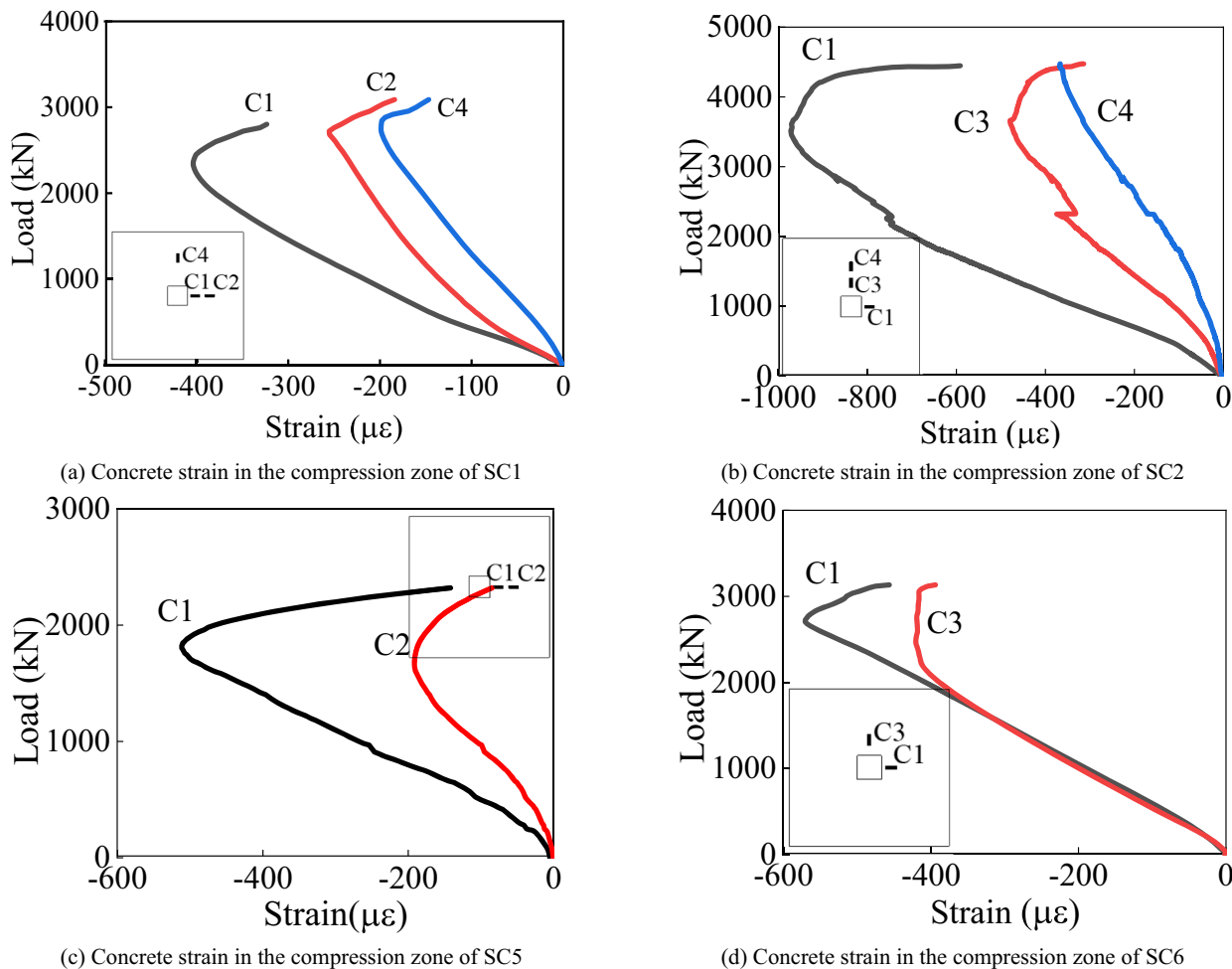


Fig. 9 Concrete strain in the compression zones of different specimens

Table 5 Specimen strain unloading situation

Specimens	Measurement points where the unloading phenomenon occurred (percentage of all measurement points)	The corresponding load percentage when the unloading phenomenon first occurred
SC1	U1, U2, U3, U4 (100%)	71.3% F_u
SC2	U1, U2, U3, U4 (100%)	63.8% F_u
SC3	U1, U2, U3 (100%)	71.0% F_u
SC4	U1, U3, U4 (100%)	81.6% F_u
SC5	U1, U2 (100%)	79.6% F_u
SC6	U1, U2 (50%)	86.2% F_u
SC7	U1 (50%)	81.4% F_u
SC8	U3, U4 (50%)	64.8% F_u
SC9	U2, U3 (50%)	75.1% F_u

complex stress state in the slab. In contrast to the specimens subjected mainly to bending failure, the specimens in

this study exhibited mainly the punch failure mode. Because the rigidity of the section steel shearhead is high, the strain of the concrete of the slab bottom is not large before the peak load. At the bottom of the slab (R1, R2, R5, and R6), the concrete is basically in a single tensile strain state, and shear forces are transferred through the interface between the reinforcement and the concrete. Tensile strain is generated on the steel bars, as shown in Fig. 10c. However, for the slab bottom position near the support (R3, R4, R7, R8), the concrete is in a composite strain state, with both tensile strain generated by bending and shear strain generated by punching. For the specimen with punching force as the main force, the latter clearly accounts for the main part, and the steel bar strain transmitted by shear force through the interface of the steel bar and concrete is very low before failure. Moreover, due to the precision error of the layout between the steel bar and section steel shearhead, it is possible for the steel bar to experience a small compressive strain or tensile strain near the failure surface. After the cracks appeared in the concrete, the longitudinal reinforcement at the bottom of the

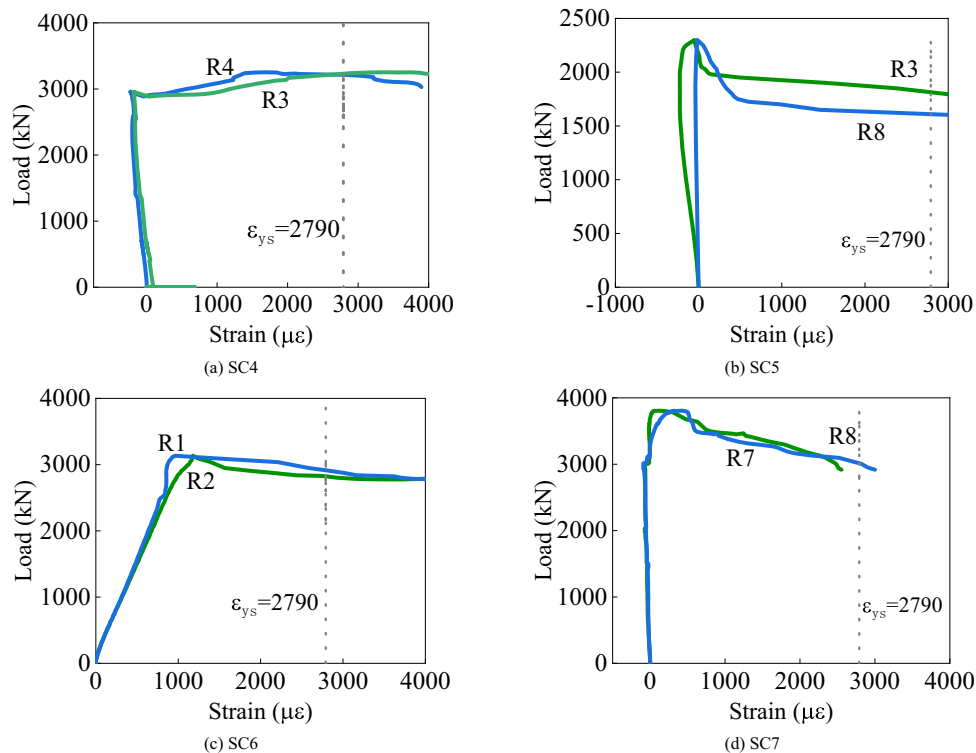


Fig. 10 Strain in the longitudinal reinforcement at the bottom of the slab

slab began to participate in the flexural resistance of the slab. Near the ultimate load, the compressive strain of the longitudinal reinforcement disappeared and was replaced by the tensile strain. When the ultimate load was reached, most of the longitudinal reinforcement at the sides of the column did not yield, the reinforcement was bonded to the concrete, which effectively inhibited the development of cracks in the slab and reduced the deformation of the slab, and the internal punching force was mainly resisted by the steel section and concrete. As the concrete in the tension zone gradually carried less of the load, the tensile strain at the rebar measurement points increased rapidly, and the strain at some measurement points reached the tensile yield strain, indicating that the longitudinal reinforcement at the bottom of the slab did not fail quickly at the later stage of loading but was able to bear its flexural capacity and work synergistically with the shearhead reinforcement. The strain at the edge of the column in specimens SC2–SC8 increased considerably with increasing load.

After reaching the ultimate load, the strain of the longitudinal reinforcement at the bottom of control specimen SC1 was quickly unloaded, and the specimen failed, far from the yield strain. In addition, in terms of the strain distribution, the strain at the column edge was very close to 300 mm from the column edge because in the absence of the shearhead, the punching shear capacity of the slab–column joint specimen was greatly reduced, which led to

the brittle punching shear failure mode, and the punching force formed a punching cone within h_0 from the edge of the column at the bottom of the slab. The specimen failed due to the crushing of the concrete in the compression zone; thus, the specimen had poor ductility, its load capacity instantly decreased at the moment of failure, and the tensile strength of the longitudinal reinforcement at the bottom of the slab was not fully exploited.

The synergistic effect of the reinforcement, steel section, and concrete was examined under the combined action of shear and bending moments. The flange thickness of specimen SC2 was excessively large, there was no flange in specimen SC5, and studs were used instead of flanges in specimen SC6. As a result, it was difficult for the steel section to work well with the longitudinal reinforcement. Due to the local failure of the concrete in the complex stress state, the slab–column joint failed before the load capacity of the steel section and longitudinal reinforcement was reached, eventually exhibiting a failure mode characterized by a combination of flexural failure and punching failure. The use of a shearhead was beneficial for providing more flexural capacity via longitudinal reinforcement at the bottom of the slab, improving the failure mode of the slab–column joint, preventing brittle punching shear failure, and increasing the ultimate load capacity and ductility of the specimen.

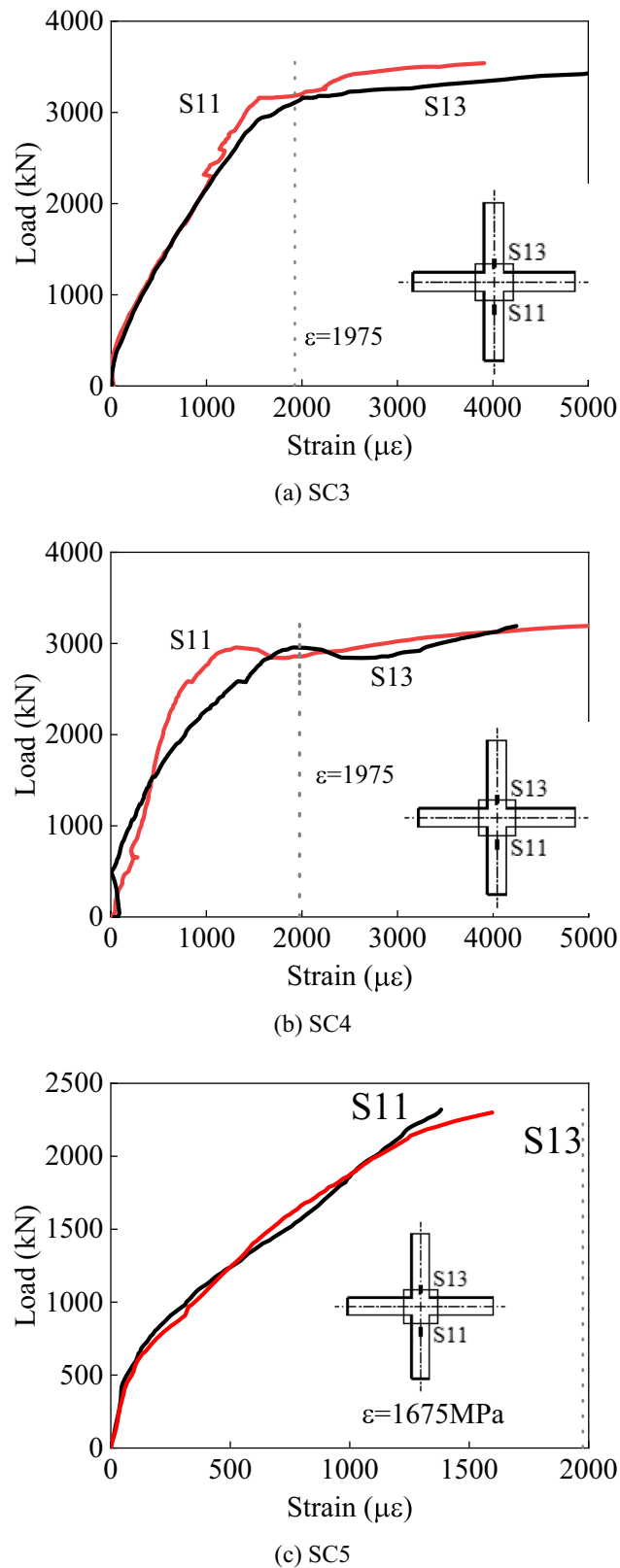


Fig. 11 Strain in the lower flange of the steel section

4.5 Strain of the Steel Section

Figure 11 shows a typical strain–load curve of the lower flange of the shearhead. After the specimen load reached 70% of the ultimate load, the tensile strain of the lower flange of the steel section increased significantly more quickly, and the tensile strain increased rapidly after reaching the ultimate load. Based on the strain development of the longitudinal reinforcement, after the ultimate load, the shearhead in the slab–column joint withstood the punching shear and worked together with the longitudinal reinforcement, which significantly improved the deformation capacity of the specimen and delayed failure. Except for those of specimens SC5 and SC9, the yield strains at the flange measurement points after the ultimate load were distributed within the range of approximately 200–300 mm from the center, indicating that the shearhead effectively participated in the flexural and shear resistance of the slab–column joint. The lower side of the web of the steel section in specimen SC5 yielded at the center point, mainly because the steel section was not provided with flanges, and as a result, the flexural stiffness was insufficient, and the concrete and the steel section did not work well together, leading to incomplete development of the shear strength of the web and the flexural–punching shear failure of the specimen due to its small flexural stiffness. Specimen SC9 had a short cantilever in the steel section; hence, the punching cone surface was expanded to the outside of the cantilever. As a result, the shearhead did not provide shear resistance, and the joint eventually underwent punching shear failure.

The analysis of the distribution of strain in the flange of the steel section revealed that the strain at the measurement points located at the edge of the column grew quickly, while the strain at the measurement points located 500–600 mm from the center of the steel section exhibited a small increase and never exceeded 30% of the yield strain. That is, the closer to the center of the steel section, the greater the tensile stress of the lower flange is due to bending, which is consistent with the pattern of deflection curves of displacement measurement points in the specimen, indicating that the shearhead not only is beneficial to the shear resistance of the slab–column joint but also contributes to its bending resistance.

The strain at each measurement point of the web of the steel section did not reach the yield level at the ultimate load. The strain of the web exhibited a complex pattern due to the shear. In the early stage of loading, the strain at most of the measurement points was small. After the concrete cracked, the strain of the web of the steel section increased. When the ultimate load was reached, the punching shear was mainly borne by the web of the steel section and the

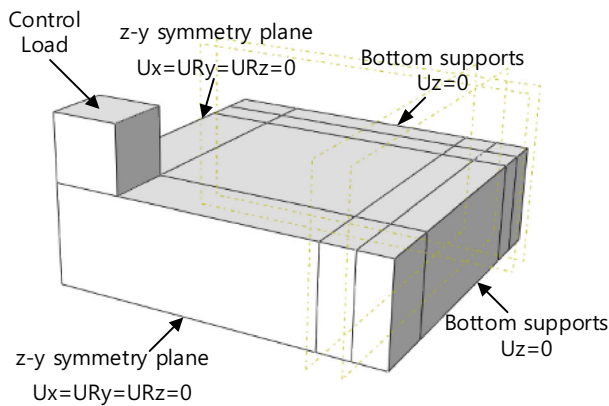


Fig. 12 Geometry and boundary conditions of the model

concrete. After the concrete in the tension zone was no longer able to withstand the load, the strain of the measurement points on the web of the steel section increased substantially until the strain measurement points failed.

5 Test Simulation and Parametric Analysis

To further study the force performance of slab–column joints with embedded shearhead reinforcement under punching shear failure, the test process was simulated using the FE software ABAQUS. The test specimen was a joint of a symmetrical slab–column structure, and only a quarter of the specimen was modeled to improve the calculation efficiency. In the model, the z-direction displacement at the slab edge was constrained to simulate the roller boundary condition, as shown in Fig. 12. The concrete damage plasticity model was used for the concrete. It was assumed that the failure mechanisms of concrete include cracking and crushing, and the constitutive model of concrete under tension–compression provided by the Chinese code GB50010-2010 was applied. A bilinear model was used for the steel; a plasticity model with a built-in von Mises yield criterion in ABAQUS was used to define the steel.

The floor slab, column, and studs were modeled by the solid element C3D8R, the shearhead by the shell element S4R, and the longitudinal reinforcement by the three-dimensional truss element T3D2. The “Embed” function was used to couple the steel and concrete and couple the longitudinal reinforcement and the concrete [29, 30]. The bond slip between the steel and concrete was considered indirectly by adjusting the “tensile hardening” parameter and the elastic modulus of the steel. A vertical load was applied to the short column with displacement control.

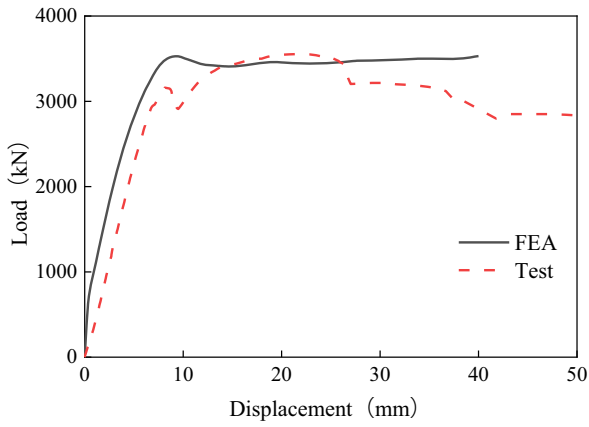
5.1 Implementation of the Numerical Model

The FE simulations were validated based on test results so that modeling parameters such as the boundary conditions, concrete fracture energy assumption, concrete dilation angle, and element mesh size were calibrated. The cross-sectional sizes, material strengths, and reinforcement of the structural members were measured. Figure 13 compares the numerical analysis results and the test results of the four typical models. The development trends of the load–deformation curves and the ultimate loads of the two are essentially comparable. The displacement and deformation of models SC3 and SC4 based on the numerical analysis results are smaller than those based on the experimental results because the FE model was based on the assumption of no bond-slip, i.e., the shearhead is considered completely embedded in concrete, and the bond effect between the steel and concrete is approximated by the expansion of tension softening. In the physical test, the stress was transferred between the concrete and the reinforcement and steel section. In general, the FE simulation results were in good overall agreement with the test results.

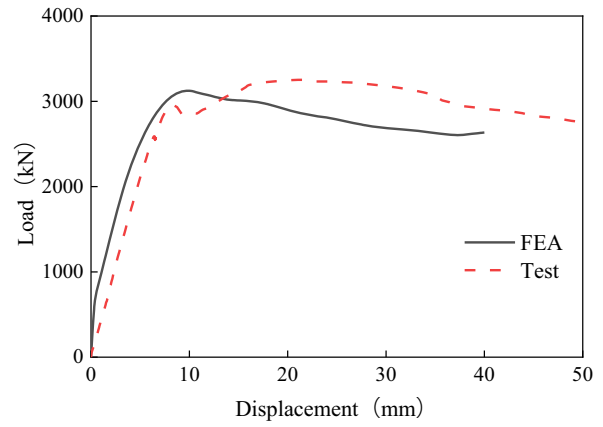
5.2 Numerical Analysis Results

5.2.1 Steel Section Deflection Curves

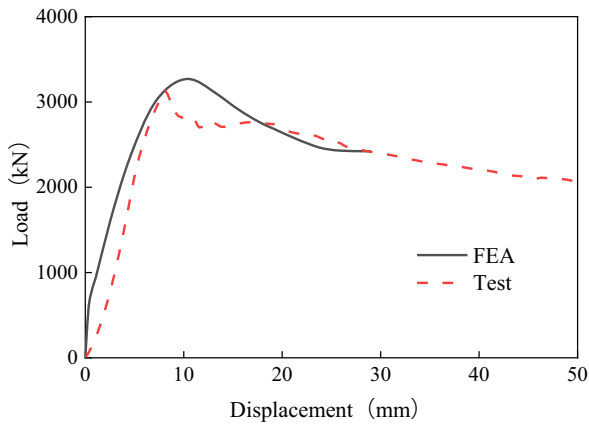
Figure 14 shows the deflection curve of the steel section when each model was loaded to the ultimate load. Figure 14a indicates that the steel section deflection of model SC5 was the smallest. As the flange thickness increased, the flexural stiffness of the steel section increased, and the deflection at the center of the slab when reaching the ultimate load also increased; therefore, the ductility of the slab–column joint improved. In Fig. 14b, due to the shortening of the cantilever in model SC9, the punching cone expanded outward along the cantilever; consequently, the steel section itself deformed only slightly, and its flexural and shear capacities were not fully utilized. Compared with model SC3, model SC7 had a greater web thickness; as the shear capacity increased, the deflection at the center of the slab under the ultimate load increased. The deflection curve of the RC slab was measured in the test, and it was found that the deflection at the mid-span of the slab in the model was essentially consistent with the test results. Between the support and the column edge, the deflection of the steel section in the model was greater than the deflection of the bottom of the slab in the test, which was attributed to the separation of the steel and concrete due to the better deformation capacity of the steel section than that of the concrete.



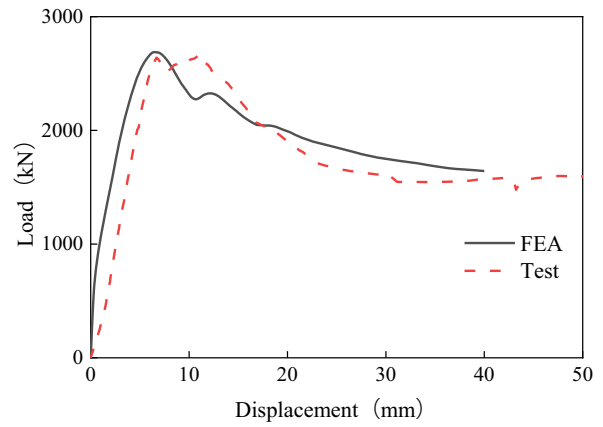
(a) SC3



(b) SC4

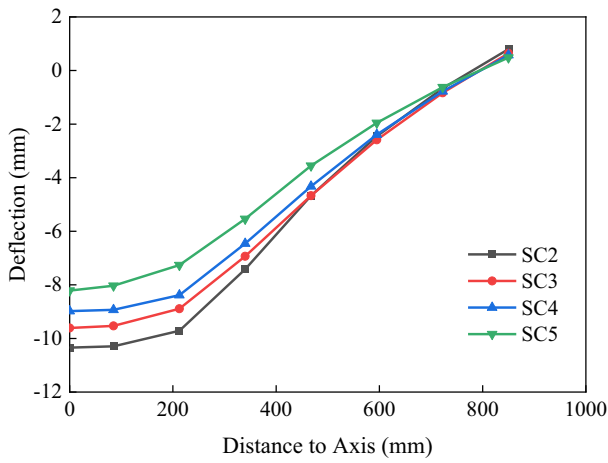


(c) SC6

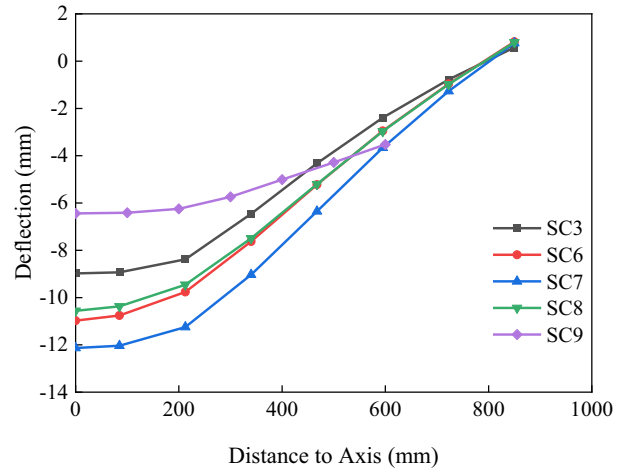


(d) SC9

Fig. 13 Load–deflection data obtained from the tests and FE analysis



(a)



(b)

Fig. 14 Steel section deflection curves of different specimens under the ultimate load

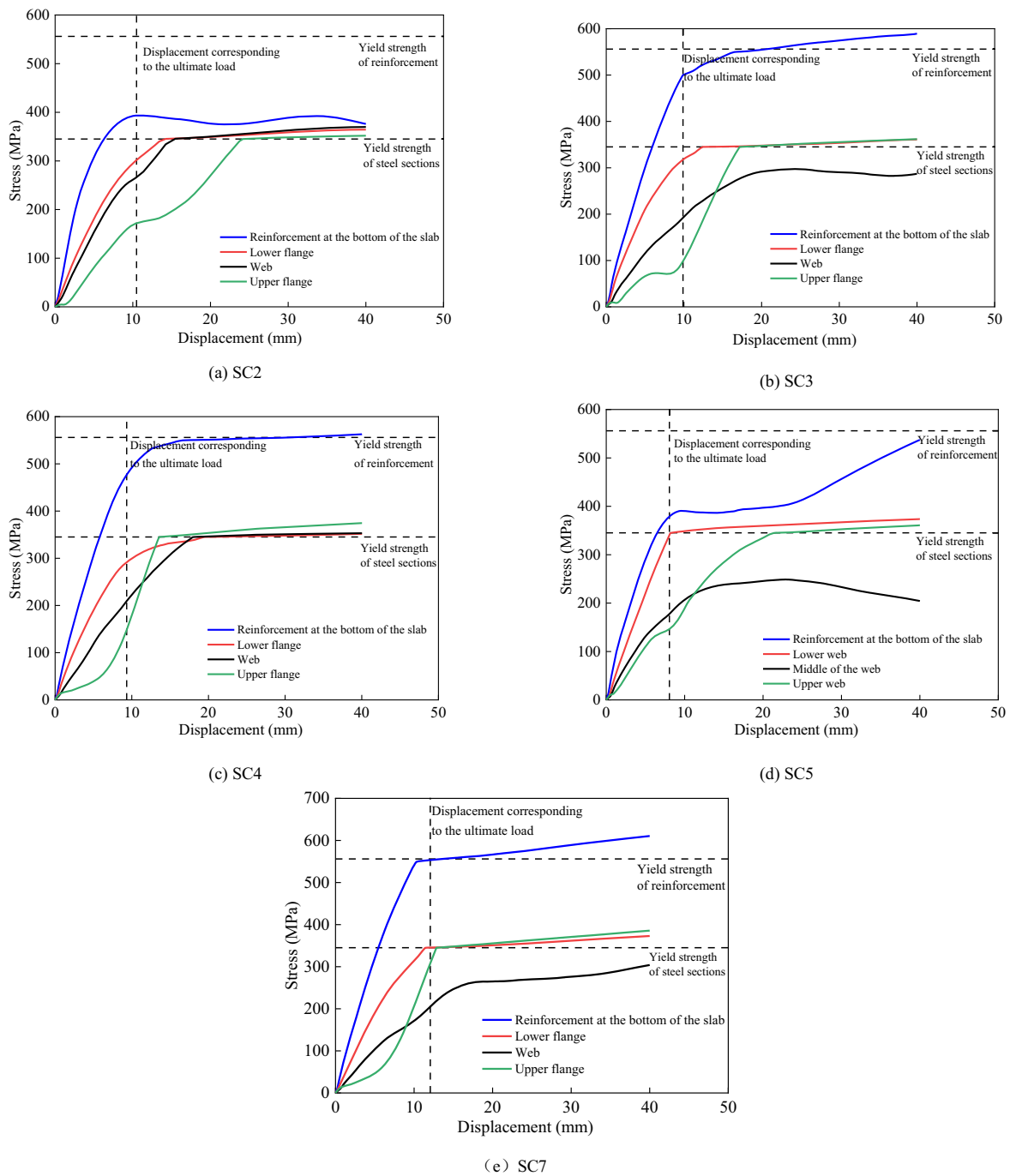


Fig. 15 Stress of each material in the section at the column edge

5.2.2 Stress Analysis

Figure 15 shows the variation in the stresses of the steel section and the reinforcement of the section at the column edge with displacement-controlled loading. When the punching load reached the maximum, the lower flange of the shearhead essentially reached the tensile yield state, while the stress level of the upper flange and the web of the

shearhead was low, and the longitudinal reinforcement at the bottom of the slab never yielded. When the load approached the maximum load, the stress curve of the upper flange of the steel section was inflected and increased rapidly. This rapid increase occurred because with further loading, the upper part of the concrete in compression was unloaded after reaching the peak compressive strain, and the stress was thus redistributed, causing part of the

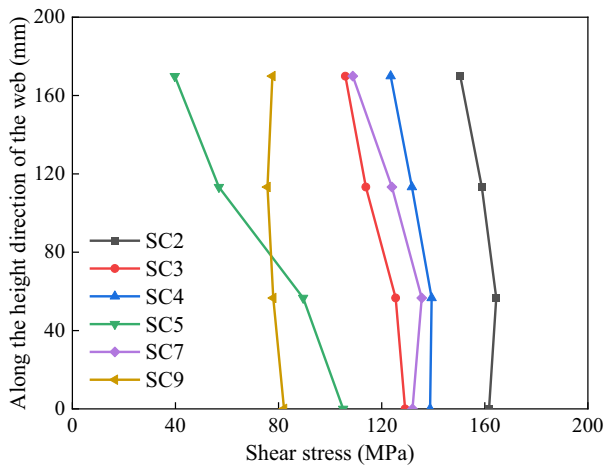


Fig. 16 Shear stress in the web section at the column edge

compressive stress originally borne by the concrete to be transferred to the upper flange plate of the steel section. After the ultimate load was reached, the stresses in the longitudinal reinforcement and the upper flange of the steel section almost stopped increasing, while the extent of damage to the concrete increased continuously; thus, the joint was no longer subjected to a greater load, and its load–deflection curve continued decreasing. The stress

variation in the steel section in the model was similar to that observed in the test, while the stress in the longitudinal reinforcement in the model did not show a small compressive strain in the early loading stage, as in the test. This difference may have occurred because the actual test results were the average values within the measurement range of the strain gauge, while the simulation results were the strain values at the element integration points; therefore, there was a certain difference in the stiffness of the curve at certain stress stages. Nevertheless, the stress variation trend and the yielding situation with increasing load were accurately simulated.

The influence of flange thickness was investigated by comparing models SC2 through SC5. Similar to the test results, after the ultimate load, the longitudinal reinforcement of models SC3 and SC4 both reached the yield stress, and the longitudinal reinforcement of model SC2 was far from yielding. This finding occurred because the thicker flange of the steel section provided greater flexural stiffness, and thus the shearhead was subjected to more bending moment than the concrete, resulting in a decrease in the bending moment for the longitudinal reinforcement at the bottom of the slab. For model SC5, which had only a web and no flange, the longitudinal reinforcement never yielded and was at a low stress level, indicating that it is difficult to

Table 6 Ultimate load depending on the thickness of the web and flange

		Ultimate load (kN)					
		Thickness of web t_1 (mm)					
		4	8	12	16	20	24
Thickness of flange t_2 (mm)	Without steel section	1968	1968	1968	1968	1968	1968
	0	2394	2519	2603	2654	2730	2763
	2	2520	2761	2822	2948	3012	3058
	4	2534	2851	2988	3120	3205	3304
	6	2581	2913	3125	3283	3375	3463
	8	2630	3006	3246	3421	3522	3605
	10	2672	3073	3336	3545	3658	3718
	12	2703	3118	3402	3667	3777	3869
	14	2731	3165	3471	3752	3903	3993
	16	2769	3217	3527	3828	3997	4115
	18	2804	3237	3576	3902	4104	4237
	20	2832	3277	3633	3958	4196	4349
	22	2872	3325	3681	4022	4279	4468
	24	2890	3366	3730	4073	4334	4561
	26	2924	3391	3760	4144	4422	4657
	28	2948	3429	3821	4195	4489	4744
	30	2982	3475	3859	4254	4570	4807
32	3013	3514	3902	4299	4622	4883	
34	3041	3549	3949	4355	4677	4962	
		Lowest	← Ultimate load →				Highest

fully utilize the strength of the longitudinal reinforcement in the presence of a steel section without a flange.

The influence of web thickness on stress was examined by comparing models SC3 and SC7. Similar to the test results, the web of model SC7 never yielded because due to the thickened web, the flexural stiffness of the steel section was not sufficient to reach the shear capacity of the web. Therefore, to increase the load capacity by thickening the web, the flange thickness should be increased accordingly.

Figure 16 shows the shear stress in the web section at the column edge of each model under the ultimate load. A comparison of models SC2, SC3, SC4, and SC5 reveals that the range and uniformity of the web stress distribution increased with increasing flange thickness. In particular, model SC5 showed a more concentrated web stress distribution than the other specimens, with a large difference in the shear stress distributed along the web and an overall smaller web shear stress than that in the other specimens with flanges, indicating that the presence of flanges may be related to the synergy of the longitudinal reinforcement, concrete, and steel section to resist punching shear.

Model SC9 had a uniform stress distribution in the web and a low stress level compared to that of the other specimens, indicating that the steel section with an overly short cantilever failed to fully exploit its shear capacity, which verified the finding that the punching cone of model SC9 expanded through the concrete instead of the steel section in the test.

5.3 Parametric Analysis

Based on the test simulation analysis model, the parameter ranges of the flange thickness and web thickness of the steel section were expanded to $0 < \text{flange}$

thickness < 34 mm and $4 \text{ mm} < \text{web thickness} < 24$ mm, respectively. Accordingly, 108 numerical models were designed to investigate the influence of different combinations of parameters. Numerical analysis of each model was conducted, with the vertical displacement controlled at a constant value of 40 mm. Table 6 shows the ultimate loads of the 108 models in two dimensions to illustrate the relationship between the two parameters considered in the study. A color scale was used to distinguish between low and high values. The lowest value of the ultimate load is shown in green, the highest value of the load is shown in orange, and the black box indicates that the model had a test control. The increase in the ultimate load capacity achieved by increasing the thickness of either the web or the flange alone was rather limited.

5.3.1 Influence of the Flange Thickness

Figure 17 shows the simulation analysis results of specimens with different flange thicknesses. Taking specimens SC2–SC5 as a reference, the web thickness of the model was kept constant at 4 mm, 8 mm, 12 mm, 16 mm, 20 mm, and 24 mm, and the flange thickness was varied from 0 to 34 mm. The variation in the mid-span displacement of each model is marked with a red dot in Fig. 17a, with the load shown in Fig. 17b.

Figure 17a indicates that the load capacity increases significantly (21.6–40.4%) with shearhead reinforcement, even by adding only the web of the shearhead without a flange in the slab–column joint. With a web thickness of 4 mm, an increase in flange thickness led to a very limited increase in the ultimate load capacity: the load capacity only increased by 20.7% as the flange was thickened from 2 to 34 mm. With a web thickness of 24 mm, increasing

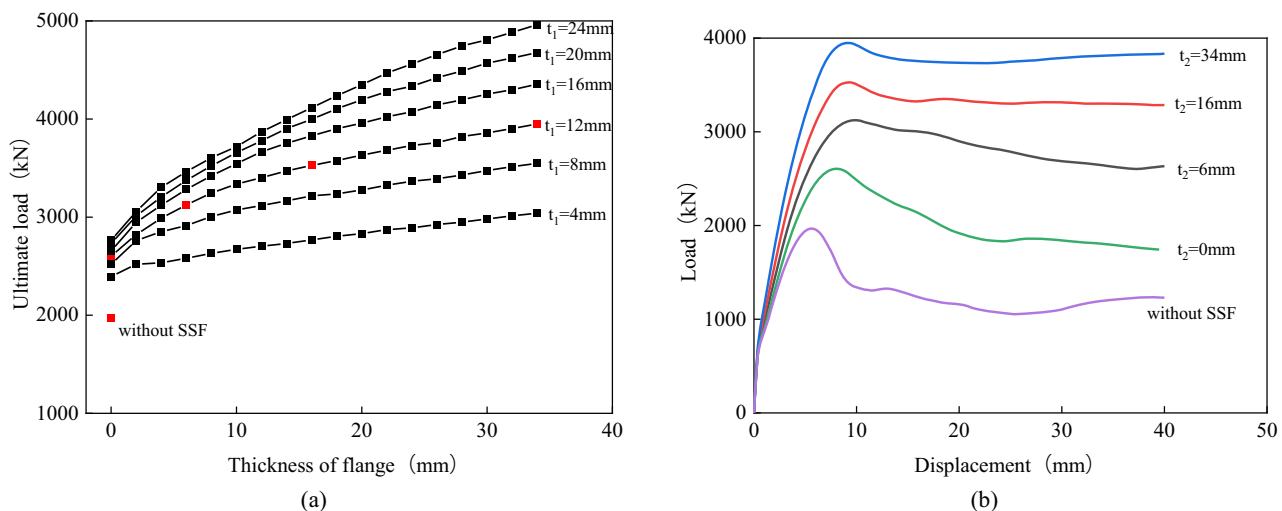


Fig. 17 Ultimate load depending on the flange thickness

the flange thickness improved the ultimate load capacity: the load capacity increased by 62.3% as the flange thickness increased from 2 to 34 mm. This result indicates that the effect of improving the ultimate load capacity by increasing the flange thickness alone was limited because the ultimate load capacity was jointly determined by the shear capacity of the web itself and the flexural stiffness of the flange.

When the flange thickness changes, the change in the ultimate load capacity can be divided into two stages. As the flange thickness increased from 2 to 10 mm, the ultimate load capacity improved with a high efficiency because the increase in flexural stiffness caused by the flange enabled the web to reach its shear capacity; in addition, the increase in the flange thickness itself led to an increase in the shear capacity. When the flange thickness increased from 12 to 34 mm, the curve in Fig. 17a was essentially linear; that is, the rate of increase in the load capacity remained essentially the same, and the increase in the ultimate load capacity was caused by the shear capacity of the flange itself. In the second stage, the approach of improving the load capacity of the joint by simply increasing the flange thickness had a certain marginal effect.

The load–displacement curves of joints without and with shearhead reinforcement are compared in Fig. 17b. The curve for the joint without a shearhead is significantly steep in the descending segment after reaching the ultimate load, indicating that the shearhead was conducive to improving the ductility of the slab–column joint. In addition, the effect of improving the ductility by using the shearhead with flanges was better than that by using the shearhead with a web only. A similar finding was obtained from the test data by comparing the load–displacement curves of

specimen SC1 and the other specimens. With the web thickness kept constant at 12 mm, the increase in the ultimate load capacity caused by increasing the flange thickness from 6 to 16 mm was similar to the increase in the ultimate load caused by increasing the flange thickness from 16 to 34 mm. These results again indicate that enhancing the load capacity of the joint by increasing the flange thickness became less effective after the flexural stiffness of the flange was sufficient for the web to reach its shear capacity.

5.3.2 Influence of the Web Thickness

Figure 18 shows the simulation analysis results of specimens with different web thicknesses. The flange thickness was kept constant at 0 mm, 6 mm, 12 mm, 18 mm, 24 mm, and 30 mm, and the web thickness was varied from 2 to 24 mm. Figure 18b shows the variation in the mid-span displacement of each model marked with a red dot in Fig. 18a with the load.

Figure 18a indicates that in the absence of flanges, the increase in the ultimate load capacity caused by thickening the web had little effect. With a flange thickness of 6 mm, the ultimate load capacity increased by 34.2% as the web thickness increased from 4 to 24 mm, and the curve became flat when the web thickness reached 12 mm. With a flange thickness of 30 mm, as the web thickness increased from 4 to 24 mm, the ultimate load capacity increased in an essentially linear manner, reaching 61.2%. This result indicates that as the flange thickness increased, the flexural stiffness of the steel section increased, as did the sensitivity of the web thickness to the ultimate load capacity. The larger the flange thickness was, the more adequate the flexural stiffness of the slab–column joint, and

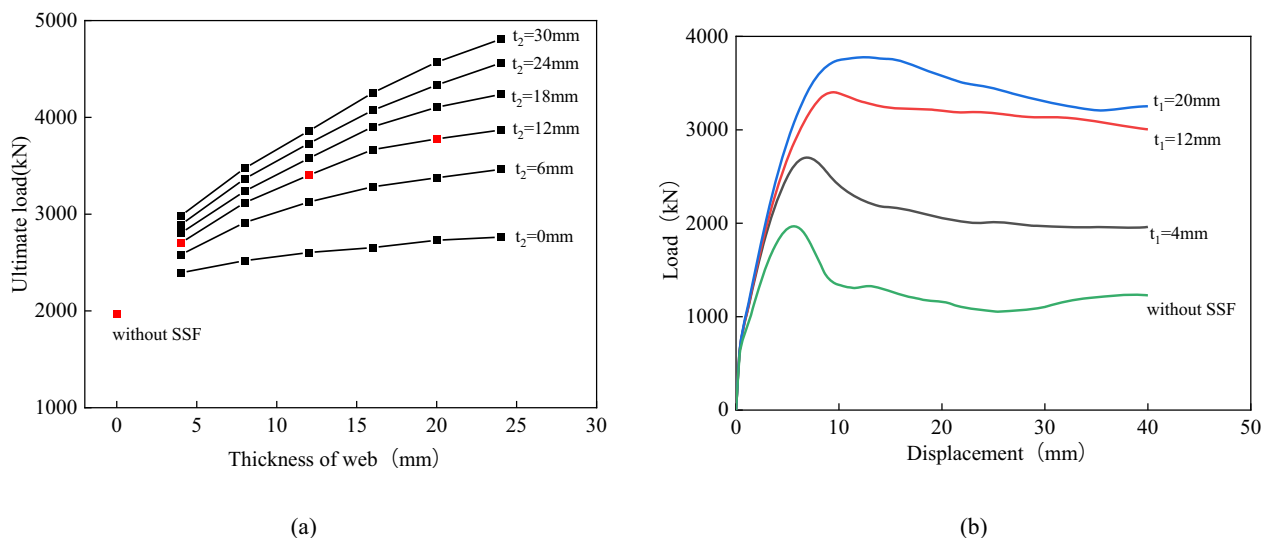


Fig. 18 Ultimate load depending on the web thickness

at this time, increasing the web thickness could effectively improve the punching shear capacity of the slab–column joint.

In Fig. 18b, the flange thickness was kept constant at 12 mm. Compared to the model without a shearhead, the increase in the web thickness improved the steep decrease in the curve after reaching the ultimate load. When the web thickness exceeded 10 mm, there was no longer a significant descending segment in the curve, which was the same for the load–deflection curves of SC2–SC8 in the test, indicating that increasing the web thickness was beneficial for improving the specimen ductility.

6 Calculation Methods for the Punching Shear Capacity

At present, there is no complete method for calculating the punching shear capacity of RC slab–column joints with shearhead reinforcement. To promote the design and application of RC slab–column joints with embedded shearheads, a set of calculation methods for punching shear capacity is proposed in this study based on the test results and numerical simulation analysis results and with reference to the relevant existing calculation methods. There are two technical improvements in the calculation method: (1) the shear capacity of the horizontal reinforcement is considered in the calculation method, which was not considered in previous studies; (2) according to the test results, the calculation of the shear capacity of the section steel is modified, the influence coefficient of the flexural stiffness of the section steel shear frame is introduced, and the factors of the flange and stud are considered. The punching shear capacity of an RC slab–column joint with an embedded shearhead is generally considered contributed by three parts, namely, the concrete (V_c), horizontal reinforcement (V_r), and steel section (V_s), as shown in Eq. (1).

$$V_T = V_c + V_r + V_s \quad (1)$$

where V_c can be calculated with reference to the empirical equations for calculating the punching shear capacity in the Chinese code GB 50010–2010 [21] or the American code ACI 318–08 [9]; the critical section perimeter is calculated based on test results; and the inclination angle θ of the punching cone surface of specimens SC2–SC8, in which the embedded steel section plays an important role, is taken as 30° (the average test result is approximately 26°). Notably, θ is taken as 45° for specimen SC1 (without steel section) according to the method in the code, and the critical section perimeter for specimen SC9 (with the shortest cantilever of the steel section) is calculated by expanding the punching cone outward to the tip of the cantilever of the steel section.

6.1 Punching Shear Capacity of Concrete

According to the Chinese code GB 50010–2010 [21], the punching shear capacity of an RC slab without stirrups or with bent-up bars under a local load or concentrated reaction force is calculated as follows:

$$V_c = 0.7\beta_h f_t \eta u_m h_0 \quad (2)$$

where β_h is the influence factor of the section height; u_m is the calculated section perimeter; h_0 is the effective height of the section; η takes the smaller of η_1 and η_2 , where η_1 is the influence factor of the shape of the area under local load or concentrated reaction force and η_2 is the influence factor of the ratio of the calculated section perimeter to the effective height of the slab section as the area under local load or concentrated reaction force; and β_s is the ratio of the long side to the short side of a rectangle.

According to the American code ACI 318–08 [9], for a slab–column joint without punching shear reinforcement, the punching shear capacity of concrete is taken as the minimum of Eqs. (3)–(5):

$$V_c = 0.083 \left(2 + \frac{4}{\beta} \right) \sqrt{f'_c} b_0 d \quad (3)$$

$$V_c = 0.083 \left(\frac{\alpha_s d}{b_0} + 2 \right) \sqrt{f'_c} b_0 d \quad (4)$$

$$V_c = 0.33 \sqrt{f'_c} b_0 d \quad (5)$$

where β is the ratio of the long side to the short side of the column section or the loading surface; f'_c is the compressive strength of the standard cylinder, $f'_c = (0.79 \sim 0.81)f_{cu,k}$, where $f_{cu,k}$ is the standard value of the concrete cube strength; b_0 is the perimeter of the critical section; d is the effective depth of the section; and α_s is the influence factor of the column position, which is taken as 40 for a center column.

6.2 Shear Capacity of the Horizontal Reinforcement

The horizontal reinforcement of the slab has a dowel effect that improves the punching shear resistance. In the limit state, the reinforcement at the bottom of the slab is essentially separated from the punching cone; therefore, its dowel effect is not considered because it cannot be reliably ensured. In contrast, the dowel effect of the longitudinal reinforcement passing through the RC column area at the top of the slab contributes to the punching shear capacity; although this part of the load capacity is generally not considered in design specifications, it should not be ignored when comparing the ultimate load capacity with the test result and is calculated as follows:

Table 7 Evaluation of the punching load capacity

Specimen	V_{test} (kN)	V_c^{GB} (kN)	V_c^{ACI} (kN)	V_r (kN)	V_s (kN)	V_{GB} (kN)	V_{ACI} (kN)	$\frac{V_{GB}}{V_{test}}$	$\frac{V_{ACI}}{V_{test}}$
SC1	3036	1641	1520	328	—	1969	1848	0.65	0.61
SC2	5079	2126	1924	328	1116	3533	3331	0.70	0.66
SC3	3555	1640	1589	328	1116	3047	2996	0.87	0.85
SC4	3252	1640	1589	328	1116	3047	2996	0.95	0.93
SC5	2336	1640	1589	328	279	2238	2187	0.96	0.94
SC6	3137	1640	1589	328	559	2454	2403	0.81	0.79
SC7	3807	1640	1589	328	1860	3766	3715	1.01	0.99
SC8	2807	1640	1589	328	837	2777	2726	1.00	0.98
SC9	2667	1931	1589	328	—	2259	1917	0.85	0.72

$$V_r = nA_s f_{vy} \quad (6)$$

where n is the number of rebars passing through the column area at the top of the RC slab and A_s is the cross-sectional area of each rebar.

6.3 Shear Capacity of the Shearhead

The aforementioned test results indicate that the shear strength of the web of the steel section was not considered independent of the flexural stiffness of the flange of the steel section. The existing codes do not consider the influence of the flexural stiffness of flanges and studs on the shear capacity. In this study, the influence factor of the flexural stiffness of the shearhead, α_f , was introduced to consider the factors of flanges and studs. According to the calculation method for the shear capacity of the oblique section of steel-RC beams in the Technical Specification for Steel-reinforced Concrete Composite Structures, JGJ 138–2001 [31], the shear capacity of the steel section can be calculated as follows:

$$V_s = \frac{4 \times 0.6 \alpha_f t_1 h_s f_{vy}}{\lambda} \quad (7)$$

where α_f is the influence factor of the flexural stiffness of the shearhead, which is set to 1 for specimens with flanges, 0.45 for specimens with studs instead of flanges, and 0.25 for specimens with neither studs nor flanges; t_1 and h_s are the slab thickness and height of the shearhead web, respectively; f_{vy} is the shear yield strength of the steel section; and λ is the shear span ratio.

6.4 Comparison of Test Results and Calculation Results

Table 7 compares the punching shear capacity calculated based on the above equation and the test results. where V_{test} is the measured punching shear capacity; V_c^{GB} and V_c^{ACI} are the concrete capacities calculated according to the two

codes; and V_{GB} and V_{ACI} are the total load capacities calculated according to the two codes.

Specimen SC1 had no steel section; the punching shear capacity was therefore provided by the concrete and the reinforcement passing through the column at the top of the slab. The ratio of the calculation result to the test result was in the range of 0.61 to 0.65, indicating the conservative prediction of the punching shear capacity of concrete in both codes. The calculation result of specimen SC2 was approximately 30% lower than the test result because the shear capacity of the thick flange of specimen SC2 was not fully considered in the calculation method. A comparison of the test results and calculation results of specimens SC3–SC9 revealed that $\frac{V_{GB}}{V_{test}}$ ranged between 0.81 and 1.01 when the concrete capacity was calculated using GB 50010–2010 [21] and that $\frac{V_{ACI}}{V_{test}}$ ranged between 0.72 and 0.99 when the concrete capacity was calculated using ACI 318–08 [9]. The above results indicate that when the flange thickness is within a certain range, the calculation method proposed in this study can effectively predict the punching shear capacity of slab–column joints with shearhead reinforcement.

7 Conclusions

The punching shear performance and failure mechanism of slab–column joints were investigated through static tests and numerical simulation analysis of nine specimens of RC slab–column joints with shearhead reinforcement. The following conclusions were drawn:

The shearhead embedded in the RC slab–column joint as a punching shear-resisting element could improve the punching shear performance of the slab–column joints, inhibit the rapid development of punching oblique cracks, withstand the internal forces released by the RC due to cracking, restrain the tensile and compressive deformation

of the concrete, and delay the formation and development of punching cones.

The nine specimens exhibited three different failure modes, namely, punching shear, flexural failure, and flexural–punching shear. A reasonable shearhead design could change the failure mode of the RC slab–column joint from brittle punching shear failure to flexural failure with a certain ductility.

The flanges of the steel section strengthened the synergy of the longitudinal reinforcement, steel, and concrete in the slab–column joint. Adding flanges and increasing the flange thickness improved the punching shear capacity and ductility of the slab–column joint to some extent. The installation of flanges on the web of the steel section increased the ultimate load capacity by more than 40% and increased the mid-span displacement at failure by more than twice that of the specimen without flanges and by that of the specimen with studs.

Adding anchor studs to the web of the steel section increased the ultimate punching shear capacity of the RC slab–column joint by 25% but did not significantly improve its deformation ductility.

A marginal effect was observed by increasing the cross-sectional area of the web to increase the load capacity. For example, the ultimate load capacity increased by only 7% when the web area increased by two-thirds. An overly short cantilever of the steel section failed to enable the shearhead to play a role in enhancing the punching shear resistance. For example, as the cantilever of the steel section was shortened from 800 to 650 mm, the ultimate load capacity was reduced by 25%, and the mid-span displacement at failure was halved.

Numerical simulations of a total of 108 FE models were conducted using the web thickness and flange thickness of the steel section as parameters. The analysis results further demonstrate that the ultimate load capacity of the joint was determined by the shear capacity of the web itself and the flexural stiffness of the flange together. Increasing the thickness of the web or flange alone was less effective at improving the ultimate load capacity.

With reference to the calculation methods for the punching shear capacity provided in existing codes, a method for calculating the punching shear capacity of RC slab–column joints with shearhead reinforcement was proposed based on tests and numerical analysis results to effectively predict the punching shear capacity of RC slabs.

The above conclusions were drawn based on the specific patterns of test results and parametric analysis results in this study. Parameters such as the RC slab thickness, reinforcement ratio, and concrete strength were within certain ranges under the constraint of test resources and thus had a limited scope of application. A wider range of parameters will be further studied in the future.

Acknowledgements The authors gratefully acknowledge the financial support from the National Nature Science Foundation of China (52378512), the Natural Science Foundation of Guangdong Province (2022A1515010878), the Foundation of the State Key Laboratory of Subtropical Building and Urban Science, South China University of Technology (2022ZA03), and the Foundation of Architectural Design & Research Institute, South China University of Technology (x2jz-D8220300).

Declarations

Conflict of interest The authors declare that they have no conflicts of interest.

References

- Foti D (2015) Shear vulnerability of historical reinforced-concrete structures. *Int J Architect Heritage* 9(4):453–467. <https://doi.org/10.1080/15583058.2013.800920>
- Ruiz MF, Muttoni A, Kunz J (2010) Strengthening of flat slabs against punching shear using post-installed shear reinforcement. *ACI Struct J* 107(4):434–442
- Isufi B, Ramos AP, Lúcio V (2019) Reversed horizontal cyclic loading tests of flat slab specimens with studs as shear reinforcement. *Struct Concr* 20(1):330–347. <https://doi.org/10.1002/suco.201800128>
- Jing Y, Yi W, Lan Hu et al (2015) Experimental study on shear performance of reinforced concrete one-way slab-column connection with shear studs. *J Build Struct* 36(8):66–72. <https://doi.org/10.14006/j.jzjgxb.2015.08.009>
- Fan JS, Bai HH, Han L et al (2021) Experimental research on punching shear behavior and calculation of bearing capacity of steel-UHPC composite slabs. *J Build Struct* 42(6):150–159. <https://doi.org/10.14006/j.jzjgxb.2019.0231>
- Dam TX, Wight JK, Parra-Montesinos GJ et al (2017) Behavior of monotonically loaded slab-column connections reinforced with shear studs. *ACI Struct J* 114(1):221–232. <https://doi.org/10.14359/51689165>
- Lips S, Ruiz MF, Muttoni A (2012) Experimental investigation on punching strength and deformation capacity of shear-reinforced slabs. *ACI Struct J* 109(6):889–900
- Bompa DV, Elghazouli AY (2017) Numerical modelling and parametric assessment of hybrid flat slabs with steel shear heads. *Eng Struct* 142:67–83. <https://doi.org/10.1016/j.engstruct.2017.03.070>
- ACI 318 (2008) Building code requirements for structural concrete and commentary. Farmington Hills: American Concrete Institute
- Bompa DV, Elghazouli AY (2016) Structural performance of RC flat slabs connected to steel columns with shear heads. *Eng Struct* 117:161–183. <https://doi.org/10.1016/j.engstruct.2016.03.022>
- Cho YS, Noh SY, Kim HW (2009) Punching shear reinforcing using studs with steel plates in reinforced concrete flat plates. *Mag Concr Res* 61(9):721–729. <https://doi.org/10.1680/mac.2008.61.9.721>
- Eder MA, Vollum RL, Elghazouli AY et al (2010) Modelling and experimental assessment of punching shear in flat slabs with shearheads. *Eng Struct* 32(12):3911–3924. <https://doi.org/10.1016/j.engstruct.2010.09.004>
- Fu CS, Lv XL, Kang J (2009) Study and design of column-supported slab and its connection. *J Build Struct* 30(2):98–106. <https://doi.org/10.14006/j.jzjgxb.2009.02.013>

14. Kim JW, Lee CH, Kang THK (2014) Shearhead reinforcement for concrete slab to concrete-filled tube column connections. *ACI Struct J* 111(3):629–638. <https://doi.org/10.14359/51686623>
15. Lee CH, Kim JW, Song JG (2008) Punching shear strength and post-punching behavior of CFT column to RC flat plate connections. *J Constr Steel Res* 64(4):418–428. <https://doi.org/10.1016/j.jcsr.2007.08.003>
16. Yan PY, Wang YC (2016) Hybrid steel tubular column/flat slab construction—development of a shearhead system to improve punching shear resistance. *J Constr Steel Res* 119:154–168. <https://doi.org/10.1016/j.jcsr.2015.12.024>
17. Navarro M, Ivorra S, Varona FB (2018) Parametric computational analysis for punching shear in RC slabs. *Eng Struct* 165:254–263. <https://doi.org/10.1016/j.engstruct.2018.03.035>
18. Marí A, Cladera A, Oller E, Bairán JM (2018) A punching shear mechanical model for reinforced concrete flat slabs with and without shear reinforcement. *Eng Struct* 166:413–426. <https://doi.org/10.1016/j.engstruct.2018.03.079>
19. Micallef K, Sagaseta J, Ruiz MF, Muttoni A (2014) Assessing punching shear failure in reinforced concrete flat slabs subjected to localised impact loading. *Int J Impact Eng* 71:17–33. <https://doi.org/10.1016/j.ijimpeng.2014.04.003>
20. Almeida AFO, Inácio MMG, Lúcio VJG, Ramos AP (2016) Punching behaviour of RC flat slabs under reversed horizontal cyclic loading. *Eng Struct* 117:204–219. <https://doi.org/10.1016/j.engstruct.2016.03.007>
21. GB 50010 (2010) Code for design of concrete structures. China Architecture and Building Press, Beijing
22. JGJ 92 (2016) Technical specification for concrete structures prestressed with unbonded tendons. China Architecture and Building Press, Beijing
23. GB/T 50081 (2002) Standard for test method of mechanical properties on ordinary concrete. China Architecture and Building Press, Beijing
24. GB/T 50152 (2012) Concrete structure test method standard. China Architecture and Building Press, Beijing
25. Yi WJ, Zhou PZ, Deng Q (2016) Experimental study of the effects of cross-sectional shape of column on punching shear performance of slab-column connection. *China Civil Eng J* 49(5):87–95. <https://doi.org/10.15951/j.tmgxcb.2016.05.008>
26. Fan J, Wang Z, Yang S (2021) Research on punching shear and bending behavior of ultra-high performance concrete slabs. *Eng Mech* 38(4):30–43
27. Dai W, Zhang Y, Qian J et al (2012) Experimental study on seismic performance of slab-column connection with shear studs under large gravity-shear ratio. *J Build Struct* 33(7):126–132. <https://doi.org/10.14006/j.jzjgxb.2012.07.015>
28. Guandalini S, Burdet O, Muttoni A (2009) Punching tests of slabs with low reinforcement ratios. *ACI Struct J* 106(1):87–95
29. Cavagnis F, Ruiz MF, Muttoni A (2015) Shear failures in reinforced concrete members without transverse reinforcement: An analysis of the critical shear crack development on the basis of test results. *Eng Struct* 103:157–173. <https://doi.org/10.1016/j.engstruct.2015.09.015>
30. Wosatko A, Pamin J, Polak MA (2015) Application of damage–plasticity models in finite element analysis of punching shear. *Comput Struct* 151:73–85. <https://doi.org/10.1016/j.compstruc.2015.01.008>
31. JGJ 138 (2001) Technical specification for steel reinforced concrete composite structures. China Architecture and Building Press, Beijing

Springer Nature or its licensor (e.g. a society or other partner) holds exclusive rights to this article under a publishing agreement with the author(s) or other rightsholder(s); author self-archiving of the accepted manuscript version of this article is solely governed by the terms of such publishing agreement and applicable law.